Gö-VIP- 22: Lukas Cyganek & Bernd Wollnik

Name der Einrichtung: Klinik für Kardiologie und Pneumologie / Stem Cell Unit sowie Institut für Humangenetik, Universitätsmedizin Göttingen

Titel der Publikation: Intronic CRISPR Repair in a Preclinical Model of Noonan Syndrome-Associated Cardiomyopathy.

In: Circulation, 6. Juli 2020, doi: 10.1161/CIRCULATIONAHA.119.044794

Autoren: Ulrich Hanses, MD[1,2†]; Mandy Kleinsorge, PhD[1,2†]; Lennart Roos, MD[1,2]; Gökhan Yigit, PhD[2,3]; Yun Li, MD[3]; Boris Barbarics, MD[2,4]; Ibrahim El-Battrawy, MD[2,5]; Huan Lan, MD[5]; Malte Tiburcy, MD[2,6]; Robin Hindmarsh, MS[1,2]; Christof Lenz, PhD[7,8]; Gabriela Salinas, PhD[3]; Sebastian Diecke, PhD[2,9,10]; Christian Müller[3]; Ibrahim Adham, PhD[3]; Janine Altmüller, MD[11]; Peter Nürnberg, PhD[11]; Thomas Paul, MD[2,4]; Wolfram-Hubertus Zimmermann, MD[2,6,12]; Gerd Hasenfuss, MD[1,2,12]; Bernd Wollnik, MD[2,3,12*]; Lukas Cyganek, PhD[1,2*]

[1]Clinic for Cardiology and Pneumology, University Medical Center Göttingen, Göttingen, Germany; [2]DZHK (German Center for Cardiovascular Research), partner site Göttingen, Mannheim and Berlin, Germany; [3]NGS Integrative Genomics Core Unit, Institute of Human Genetics, University Medical Center Göttingen, Göttingen, Germany; [4]Clinic for Pediatric Cardiology and Intensive Care Medicine, University Medical Center Göttingen, Göttingen, Germany; [5]First Department of Medicine, Medical Faculty Mannheim, University Medical Centre Mannheim, University of Heidelberg, Mannheim, Germany; [6]Institute of Pharmacology and Toxicology, University Medical Center Göttingen, Göttingen, Germany; [7]Institute for Clinical Chemistry, University Medical Center Göttingen, Göttingen, Germany; [8]Bioanalytical Mass Spectrometry, Max Planck Institute for Biophysical Chemistry, Göttingen, Germany; [9]Stem Cell Core Facility, Max Delbrück Center for Molecular Medicine, Berlin, Germany; [10]Berlin Institute of Health, Berlin, Germany; [11]Cologne Center for Genomics, University of Cologne, Cologne, Germany; [12]Cluster of Excellence "Multiscale Bioimaging: from Molecular Machines to Networks of Excitable Cells" (MBExC), University of Göttingen, Göttingen, Germany

[†]These authors contributed equally to this work.

*Co-corresponding authors

Zusammenfassung des wissenschaftlichen Inhalts

(Lukas Cyganek & Bernd Wollnik)

Das Noonan-Syndrom ist eine Erbkrankheit, die mit Entwicklungsstörungen einhergeht und verschiedene Symptome aufweisen kann: Wachstumsverzögerung, Kleinwuchs, Fehlbildungen des Gesichts, sowie – vor allem klinisch bedeutsam – schwerwiegende Herzfehler. Zugrundeliegende Mutationen bewirken eine Überaktivierung des RAS-MAP-Kinase-Signalwegs, jedoch sind die Zusammenhänge zwischen den jeweiligen Genmutationen und der Ausbildung von Herzfehlern (wie einer Hypertrophie) noch nicht vollständig aufgeklärt und daher auch die Behandlungsmöglichkeiten stark limitiert.

In dieser Studie konnten in zwei betroffenen Brüdern mit sehr schweren Ausprägungen der Hypertrophie compound-heterozygote Mutationen im LZTR1-Gen (leucine zipper like transcription regulator 1) in rezessiver Form als Ursache identifiziert werden. Hautzellen von beiden Kindern wurden zu induzierten pluripotenten Stammzellen (iPS-Zellen) reprogrammiert, welche anschließend in Herzmuskelzellen (iPSC-Kardiomyozyten) differenziert und auf molekularer wie auch funktioneller Ebene untersucht wurden. Wir konnten zeigen, dass die patientenspezifischen iPSC-Kardiomyozyten den pathologischen hypertrophen Phänotyp rekapitulieren und eine molekulare Signatur der Erkrankung erstellen. Hierdurch wurde ein kausaler Link zwischen LZTR1 Dysfunktion, RAS-MAPK Hyperaktivierung, hypertropher Gen-Antwort und zellulärer Hypertrophie aufgedeckt. Wir konnten außerdem zeigen, dass eine medikamentöse Therapie (Calcium-Kanal-Blocker oder Inhibition des RAS-MAPK-Signalwegs) nur bedingt gegen die Symptome in den iPSC-Kardiomyozyten hilft. Die intronische Genkorrektur mittels CRISPR/Cas9 in den patientenspezifischen iPS-Zellen beider Kinder konnte den Krankheits-Phänotyp (vor allem: Normalisierung der Signalwegs-Aktivität und der Hypertrophie) beheben und somit als eine personalisierte und klinisch-übertragbare Behandlungsstrategie identifiziert werden.

Weitere Informationen:
Universitätsmedizin Göttingen
Klinik für Kardiologie und Pneumologie / Stem Cell Unit
Dr. Lukas Cyganek, Telefon: 0551/ 39 64280
Robert-Koch-Str. 40, 37075 Göttingen
lukas.cyganek@gwdg.de

Universitätsmedizin Göttingen
Institut für Humangenetik
Prof. Dr. Bernd Wollnik, Telefon: 0551/ 39 67589
Heinrich-Düker-Weg 12, 37073 Göttingen
bernd.wollnik@med.uni-goettingen.de

Circulation

ORIGINAL RESEARCH ARTICLE

Intronic CRISPR Repair in a Preclinical Model of Noonan Syndrome–Associated Cardiomyopathy

BACKGROUND: Noonan syndrome (NS) is a multisystemic developmental disorder characterized by common, clinically variable symptoms, such as typical facial dysmorphisms, short stature, developmental delay, intellectual disability as well as cardiac hypertrophy. The underlying mechanism is a gain-of-function of the RAS–mitogen-activated protein kinase signaling pathway. However, our understanding of the pathophysiological alterations and mechanisms, especially of the associated cardiomyopathy, remains limited and effective therapeutic options are lacking.

METHODS: Here, we present a family with two siblings displaying an autosomal recessive form of NS with massive hypertrophic cardiomyopathy as clinically the most prevalent symptom caused by biallelic mutations within the leucine zipper-like transcription regulator 1 (*LZTR1*). We generated induced pluripotent stem cell–derived cardiomyocytes of the affected siblings and investigated the patient-specific cardiomyocytes on the molecular and functional level.

RESULTS: Patients' induced pluripotent stem cell–derived cardiomyocytes recapitulated the hypertrophic phenotype and uncovered a so-far-not-described causal link between LZTR1 dysfunction, RAS–mitogen-activated protein kinase signaling hyperactivity, hypertrophic gene response and cellular hypertrophy. Calcium channel blockade and MEK inhibition could prevent some of the disease characteristics, providing a molecular underpinning for the clinical use of these drugs in patients with NS, but might not be a sustainable therapeutic option. In a proof-of-concept approach, we explored a clinically translatable intronic CRISPR (clustered regularly interspaced short palindromic repeats) repair and demonstrated a rescue of the hypertrophic phenotype.

CONCLUSIONS: Our study revealed the human cardiac pathogenesis in patient-specific induced pluripotent stem cell–derived cardiomyocytes from NS patients carrying biallelic variants in *LZTR1* and identified a unique disease-specific proteome signature. In addition, we identified the intronic CRISPR repair as a personalized and in our view clinically translatable therapeutic strategy to treat NS-associated hypertrophic cardiomyopathy.

Ulrich Hanses, MD*
Mandy Kleinsorge, PhD*
⋮
Lukas Cyganek, PhD

*Drs Hanses and Kleinsorge contributed equally.

The full author list is available on page 1074.

Key Words: cardiomyopathy, hypertrophic ■ clustered regularly interspaced short palindromic repeats ■ gene editing ■ induced pluripotent stem cells ■ Noonan syndrome

Sources of Funding, see page 1074

https://www.ahajournals.org/journal/circ

Clinical Perspective

What Is New?

- The authors found that biallelic mutations in *LZTR1* confer a high risk for the development of hypertrophic cardiomyopathy in patients with Noonan syndrome.
- The authors show that *LZTR1*-deficient induced pluripotent stem cell–cardiomyocytes from Noonan syndrome patients recapitulate the hypertrophic phenotype with evidence of abnormal calcium handling as a contributor to the clinical disease phenotype.
- Molecular and functional phenotyping identified a unique disease-specific proteome signature and provided a causal link between LZTR1 dysfunction, RAS–mitogen-activated protein kinase signaling hyperactivity, hypertrophic gene response, and cellular hypertrophy.

What Are the Clinical Implications?

- Patient-specific induced pluripotent stem cell–cardiomyocytes can be used as a preclinical model of Noonan syndrome–associated cardiomyopathy to assess novel therapeutic approaches.
- L-type calcium channel blockade and MEK inhibition could prevent some of the disease characteristics in the patients' induced pluripotent stem cell cardiomyocytes, such as normalization of calcium homeostasis and RAS–mitogen-activated protein kinase signaling activity, respectively, providing a molecular underpinning for the clinical use of these drugs in patients with Noonan syndrome, but might not be a sustainable therapeutic option.
- Intronic CRISPR repair rescued the hypertrophic phenotype in the patients' induced pluripotent stem cell–cardiomyocytes, thereby revealing a personalized and in our view clinically translatable strategy for therapeutic genome editing.

Noonan syndrome (NS) is a monogenic developmental disorder that is characterized by typical facial dysmorphisms, webbing of the neck, short stature with relative macrocephaly, skin and hair affections, developmental delay, intellectual disability, as well as an increased tumor predisposition. Congenital heart disease is commonly observed and typically presents as pulmonary valve stenosis, atrial, or ventricular septum defect, and early-onset hypertrophic cardiomyopathy (HCM).[1] With a prevalence of 1 in 1000 to 2500 live births NS is one of the most common genetic diseases associated with congenital heart defects and especially early-onset HCM.[2,3] Infants with HCM as a symptom of NS are more likely to develop heart failure and display a significantly worse late survival compared with patients with isolated, nonsyndromic HCM.[4,5] NS belongs to the spectrum of RASopathies and is associated with mutations in several genes leading to an increased signal activation and transduction along the RAS–mitogen-activated protein kinase (MAPK) signaling pathway.[6,7] Autosomal dominant mutations in genes encoding components or regulators of the RAS-MAPK pathway that have been described so far, including *PTPN11*,[8] *SOS1*,[9] *RAF1*,[10,11] *RIT1*,[12] *KRAS*,[13] *NRAS*,[14] *RRAS*,[15] *SHOC2*,[16] *PPP1CB*,[17] and *CBL*,[18] account for >90% of all classical NS cases.[19] In addition to their association with schwannomatosis[20] and glioblastoma,[21] autosomal dominant missense mutations, as well as autosomal recessive biallelic mutations in leucine zipper-like transcription regulator 1 (*LZTR1*) were linked to NS.[22,23] Recent studies verified the cellular function of LZTR1 as an adaptor for the cullin 3 ubiquitin ligase complex and identified RAS proteins as its direct targets for degradation.[24–26] However, the molecular pathogenesis, especially of the associated cardiomyopathy, is largely unknown and the link between RAS-MAPK signaling dysfunction and the often very early manifestation of the cardiomyopathy remains unclear. Interestingly, the presence and severity of HCM seems to be genotype-dependent, with HCM being more often associated with mutations in *RAF1, RIT1,* and *LZTR1*.[10,12,23] Despite the epidemiological relevance of NS, disease-specific pharmacological as well as invasive therapy options remain limited, and no curative treatment exists.

The development of induced pluripotent stem cell (iPSC) technology allows to study human disease using patient-specific cells in vitro.[27] So far, few RASopathy-related human iPSC models have been established (eg, for NS,[28] NS with multiple lentigines,[29] Costello syndrome,[30] and cardiofaciocutaneous syndrome[31]). Substantial evidence shows that iPSC-derivatives, like iPSC-derived cardiomyocytes (iPSC-CMs), from patients with genetic disorders represent the phenotype of the disease, thereby providing a powerful platform for modeling genetic diseases, investigating the underlying pathological mechanisms and for testing of novel therapeutic approaches.[32,33] Moreover, the recent advent of CRISPR (clustered regularly interspaced short palindromic repeats)/Cas9–mediated genome editing not only fundamentally enriched biomedical research, but also redefined precision medicine by offering new therapeutic perspectives for the treatment of genetically inherited cardiovascular diseases.[34,35]

In this study, we present a family with 2 siblings displaying an autosomal recessive form of NS with severe HCM with outflow obstruction caused by compound heterozygous mutations within *LZTR1*. We generated iPSCs of the affected siblings and investigated the patient-specific iPSC-CMs on the molecular, cell biological and functional level. The patient-specific iPSC-CMs recapitulated the hypertrophic phenotype in vitro and uncovered a causal link between LZTR1 dysfunction,

RAS accumulation, RAS-MAPK signaling hyperactivity, hypertrophic gene response and cellular hypertrophy. In addition, intron editing was explored to normalize RAS-MAPK signaling activity and cellular hypertrophy, thereby revealing a personalized and in our view clinically translatable therapeutic strategy.

METHODS

An extended methods section is available in the Data Supplement. All data, methods used in the analysis, and human iPSC lines deposited in the Biobank of the University Medical Center Göttingen are available to other researchers on request.

Ethical Approval

The study was approved by the Ethics Committee of the University Medical Center Göttingen (approval number: 10/9/15) and carried out in accordance with the approved guidelines. Written informed consent was obtained from all participants or their legal representatives before participation in the study and for publishing identifiable images.

Human iPSCs

Human iPSC lines from 2 patients diagnosed with NS and 3 healthy donors were used in this study. Human iPSC lines iBM76.1 (UMGi005-A.1; here abbreviated as WT1) and iWT.D2.1 (UMGi001-A.1; here abbreviated as WT3) were generated from mesenchymal stem cells and dermal fibroblasts, respectively, using the STEMCCA lentivirus system and described previously.[36] Human iPSC line ipWT1.3 (UMGi014-B.3; here abbreviated as WT2) was generated from dermal fibroblasts using an integration-free episomal reprogramming plasmid and described previously.[37] Human iPSC lines isHOCMx1.14 (UMGi030-A.14; here abbreviated as NS1-1), isHOCMx1.16 (UMGi030-A.16; here abbreviated as NS1-2), isHOCMx2.3 (UMGi031-A.3; here abbreviated as NS2-1) and isHOCMx2.8 (UMGi031-A.8; here abbreviated as NS2-2) were generated from dermal fibroblasts from the index patients II_1 and II_2 using the integration-free CytoTune-iPS 2.0 Sendai Reprogramming kit (Thermo Fisher Scientific) according to manufacturer's instructions with modifications. The iPSC lines isHOCMx1.14 and isHOCMx2.3 were used for CRISPR/Cas9-mediated genetic correction and 4 CRISPR-repaired iPSC lines were selected, isHOCMx1-corr.4 (UMGi030-A-1.4, here abbreviated as NS1-corr1) and isHOCMx1-corr.34 (UMGi030-A-1.34, here abbreviated as NS1-corr2) for patient II_1, and isHOCMx2-corr.2 (UMGi031-A-1.2, here abbreviated as NS2-corr1) and isHOCMx2-corr.33 (UMGi030-A-1.33, here abbreviated as NS2-corr2) for patient II_2.

Characterization of iPSC-Derived Cardiomyocytes

Directed differentiation of iPSCs into iPSC-CMs was performed via WNT signaling modulation and subsequent metabolic selection, as previously described.[36] iPSC-CMs were cultured for 2 to 3 months and subjected to molecular and functional analyses.

RNA Sequencing and Mass Spectrometry Proteomics

RNA sequencing data are available at the National Center for Biotechnology Information's Gene Expression Omnibus (http://www.ncbi.nlm.nih.gov/geo/) under accession number GSE145350. Mass spectrometry proteomics data are available via the PRIDE partner repository ProteomeXchange (http://www.proteomexchange.org) with identifier PXD017530.

Statistical Analysis

Data are presented as the mean±SEM unless otherwise specified. Statistical comparisons were performed using the D'Agostino-Pearson normality test and the nonparametric unpaired and 2-tailed Mann-Whitney test, the nonparametric Kruskal-Wallis test followed by Dunn correction or the nonparametric 1-sample Wilcoxon test using GraphPad Prism 8. Results were considered statistically significant when the P value was <0.05 (*P<0.05; **P<0.01; ***P<0.001; ****P<0.0001; not significant, P>0.05).

RESULTS

Biallelic Mutations in LZTR1 Cause Noonan Syndrome

We have identified and clinically characterized a nonconsanguineous family with 2 affected boys diagnosed with NS (Figure 1A). Strikingly, both siblings, currently 7 and 4 years of age, presented with a very early-onset form of hypertrophic obstructive cardiomyopathy, which was diagnosed by echocardiography (Figure 1B, Figure I in the Data Supplement, and Table I in the Data Supplement). In addition, both siblings presented with a typical facial dysmorphism (Figure 1C), webbing of the neck, developmental delay, and short stature with relative macrocephaly (Table II in the Data Supplement). Because of the severity and the early onset of hypertrophy, both children underwent septal myectomy including cardioverter-defibrillator implantation at the age of 3.5 years and 6 months, respectively, to recover cardiac function and to prevent sudden cardiac death.

Routine molecular diagnostic testing of NS-associated genes by next generation sequencing-based multigene panel analysis did not reveal a causative mutation. Subsequently, we performed whole-exome sequencing and detected one interesting heterozygous variant in both brothers, the c.27dupG variant in *LZTR1*, which is predicted to cause a frameshift and a premature truncation of the protein (p.Q10Afs*24). Family analysis revealed that this variant was inherited from the healthy mother (Figure 1D and 1E). Further in-depth analysis detected an additional deep-intronic variant in *LZTR1* in both siblings, namely c.1943-256C>T. This paternally inherited variant is located in intron 16 and predicted to create an additional donor splice site (Figure 1D and 1E).

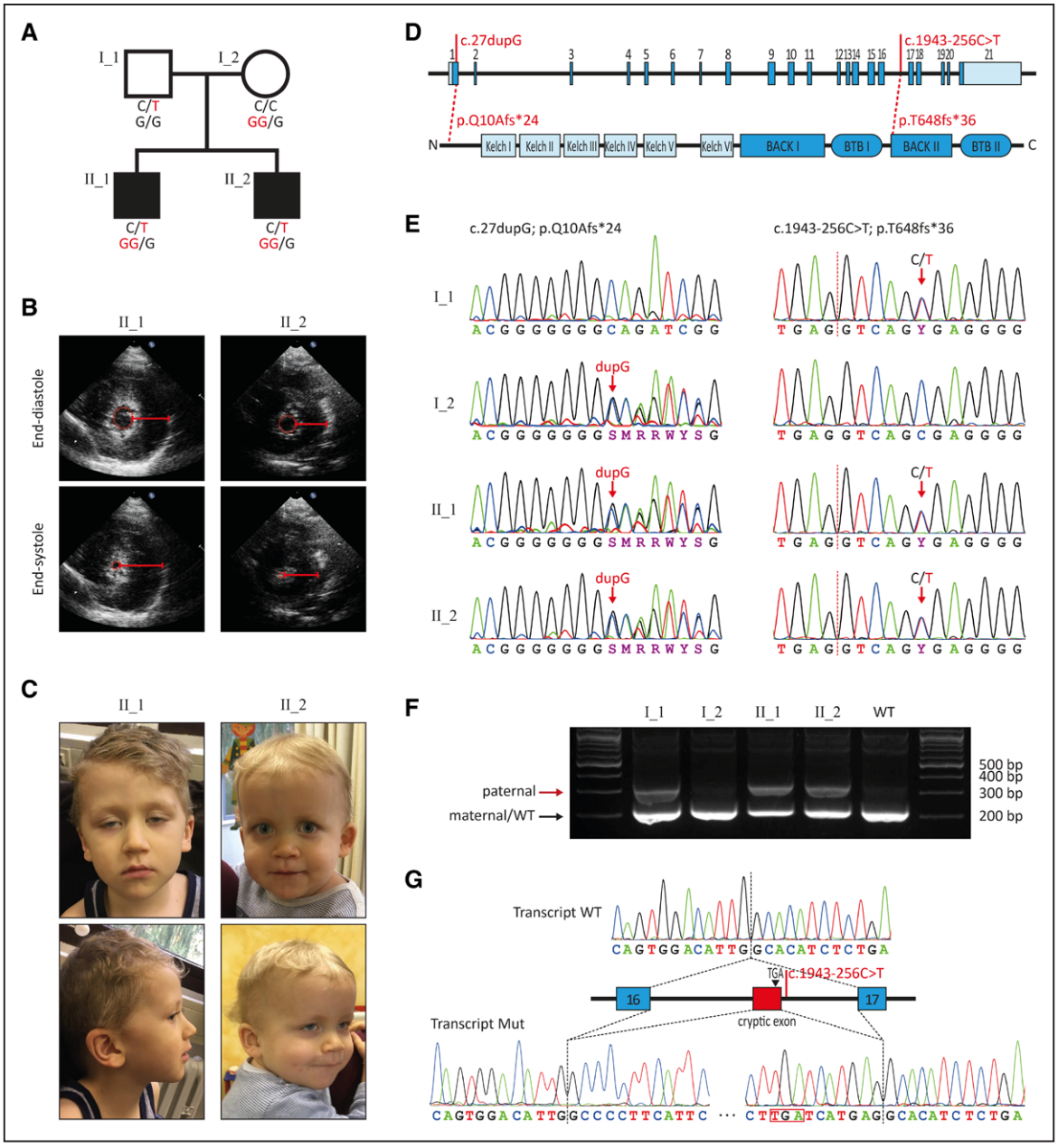

Figure 1. Biallelic mutations in LZTR1 cause Noonan syndrome.
A, Pedigree of the affected family showing the healthy parents (father I_1 and mother I_2) and the afflicted siblings (II_1 and II_2). **B**, Echocardiogram in the parasternal short-axis view of both brothers at the age of 3.5 years (II_1) and 6 months (II_2) before surgical intervention. The left ventricle displayed in diastole and systole demonstrated a severely hypertrophic myocardium (red lines). **C**, Facial features of the affected siblings at the age of 5 years (II_1) and 2 years (II_2). Siblings presented with Noonan syndrome–typical facial dysmorphism including hypertelorism, frontal bossing, ptosis, low-set ears, and short neck. **D**, Overview of the identified compound heterozygous mutations in *LZTR1* on genomic and protein level, and (**E**) Sanger sequencing of exon 1 and intron 16 in all 4 family members. The maternal mutation c.27dupG in exon 1 is predicted to cause a frameshift and an early termination of protein synthesis (p.Q10Afs*24). The paternal mutation c.1943-256C>T in intron 16 introduces an additional donor splice site which leads to the inclusion of a cryptic exon in the *LZTR1* transcript and is predicted to result in a truncated protein. Both siblings (II_1 and II_2) present both biallelic mutations in *LZTR1*. **F**, The inclusion of the additional cryptic exon between exons 16 and 17 was detectable on mRNA level in iPSC samples of the father (I_1) and the siblings (II_1 and II_2), displaying an additional 117 bps larger band, assessed by reverse transcriptase polymerase chain reaction. No mutational transcript was detectable in samples of the mother (I_2) and a healthy WT donor. **G**, Sanger sequencing of the *LZTR1* transcript in exons 16 to 17 confirmed the bioinformatics predictions. Compared with the maternal allele, the paternal new splice donor c.1943-256C>T in intron 16 resulted in the inclusion of a cryptic exon between exons 16 and 17, which possesses a premature stop codon (TGA) sequence. WT indicates wild type.

The cDNA analysis from patient samples confirmed the effect of the c.1943-256C>T variant on splicing of the *LZTR1* transcripts (Figure 1F), with the paternal transcript being selectively targeted for nonsense-mediated mRNA decay (Figure II in the Data Supplement).[38] The introduction of a new splice donor by the variant—in combination with a potential acceptor splice site in the neighborhood—leads to the recognition of an aberrant, cryptic exon between exon 16 and exon 17, which is included into the transcript (Figure 1G). This 117 bps cryptic

exon includes a stop codon, which was predicted to cause a premature truncation of the protein (p.T648fs*36). The identical intronic mutation has also been observed in unrelated patients described recently.[23] As a result of the compound heterozygous mutations in *LZTR1*, it is unlikely that sufficiently functional LZTR1 is translated.

Patient-Specific Cardiomyocytes Recapitulate the Hypertrophic Disease Phenotype

To elucidate the consequences of the identified biallelic *LZTR1* mutations on CM morphology and function, we generated iPSCs from skin biopsies of both siblings (II_1 and II_2) using nonintegrating reprogramming methods. A minimum of 6 individual iPSC lines per patient displaying a typical stem cell-like morphology were established and 2 iPSC lines per patient, denoted as NS1-1 and NS1-2 from index patient II_1 and NS2-1 and NS2-2 from index patient II_2, were selected for detailed pluripotency analysis (Figure IIIA through IIIF in the Data Supplement). The presence of the compound heterozygous mutations c.27dupG and c.1943-256C>T in *LZTR1* in the patient-specific iPSC lines was confirmed by Sanger sequencing on genomic as well as on transcriptional level (Figure IIIG and IIIH in the Data Supplement). The iPSC lines WT1, WT2 and WT3 from 3 healthy donors, which were used as wild type (WT) controls in this study, were negative for the respective mutations in *LZTR1* (Figure IIIG in the Data Supplement).

The patient-specific iPSC lines from both siblings as well as 3 individual WT controls were differentiated into functional, predominantly ventricular-like, iPSC-CMs in feeder-free culture conditions[36] to model the clinically observed ventricular hypertrophy phenotype. Multiple iPSC lines from WT and NS were investigated for potential phenotypic variability: spontaneously contracting areas appeared between days 8 to 10 of differentiation in all iPSC lines and no differences in the differentiation efficiency were observed between mutant and control iPSC lines. The CM purity of the cultures was determined by flow cytometry and resulted in >94% α-actinin$^+$ iPSC-CMs in NS cultures and WT controls (Figure 2A). The CM cultures derived from both NS and control iPSCs showed robust expression of cardiac-specific genes α-actinin (*ACTN2*), cardiac troponin T (*TNNT2*), ventricular-restricted myosin light chain 2 V (*MYL2*), connexin 43 (*GJA1*) and *NKX2-5* at similar levels (Figure 2B). Atrial natriuretic factor (*NPPA*) and brain natriuretic peptide (*NPPB*), whose induction is often associated with hypertrophy,[39] were not upregulated in NS cultures (Figure 2B). Interestingly, genes responsible for calcium handling such as ryanodine receptor 2 (*RYR2*) and ATPase sarcoplasmic/endoplasmic reticulum calcium transporting 2 (*ATP2A2*) were significantly upregulated in NS cultures, suggesting differences in calcium homeostasis (Figure 2B). Besides its expression in undifferentiated iPSCs, the *LZTR1* transcript was also present in the differentiated iPSC-CMs of all cell lines implying its role in cardiac development and function (Figure 2B). Immunocytochemical staining of cardiac subtype-specific proteins revealed that both the patient-derived iPSC-CMs and the control iPSC-CMs exhibit a well-organized sarcomeric organization visualized by α-actinin and ventricular-specific MLC2V (Figure 2C). Furthermore, a pronounced striated expression of the sarcoplasmic reticulum calcium channel RYR2 was observed indicating proper localization of the calcium release units (Figure 2D).

To determine whether the NS patients' iPSC-CMs display a hypertrophic phenotype, cells were analyzed for their size. Since cell size is highly dependent on cell density, the iPSC-CMs were digested and plated in various densities on a 12-well plate, from a highly confluent monolayer to sparse 2D culture, allowing the determination of cell size distribution as a function of CM confluency (Figure 2E). After ten days of recovery, the iPSC-CMs of all 4 NS iPSC lines, as well as 3 WT iPSC lines, were first analyzed for cell area in adherent culture, and secondly, singularized and analyzed for cell diameter in suspension to confirm the optical findings. Both assays concordantly (1) confirmed that, in agreement with other models, CM size in culture is closely related to cell density and (2) demonstrated a larger size of iPSC-CMs from NS patients compared with WT iPSC-CMs under low-density culture conditions (Figure 2F through 2I).

Collectively, these data demonstrated that the iPSC-CMs from the NS patients efficiently differentiate into well-organized, functional CMs and recapitulate the hypertrophic phenotype in vitro.

Patient-Specific Cardiomyocytes Display Altered Calcium Homeostasis

Subsequently, we investigated the contractile function and rhythmogenesis of CM cultures from NS patients by automated video analysis[40] and multielectrode array. Whereas no differences in the contraction and relaxation times were observed (Figure 3A through 3C), the contraction amplitude (measured by impedance change) was increased in the patients' iPSC-CMs (Figure 3D), implying a higher force generation. The field potential duration and the conduction velocity were unchanged in comparison to controls (Figure 3E through 3G). Although the beat-to-beat variability was modestly lower in the control group, both NS and WT cultures displayed a high degree of beat regularity (Figure 3H).

Motivated by the observed differences in the expression of calcium handling genes and their implied influence on CM electrophysiology, we examined action potential (AP) kinetics in iPSC-CMs by patch-clamping (Figure 3I). AP duration at 50% repolarization, which is determined

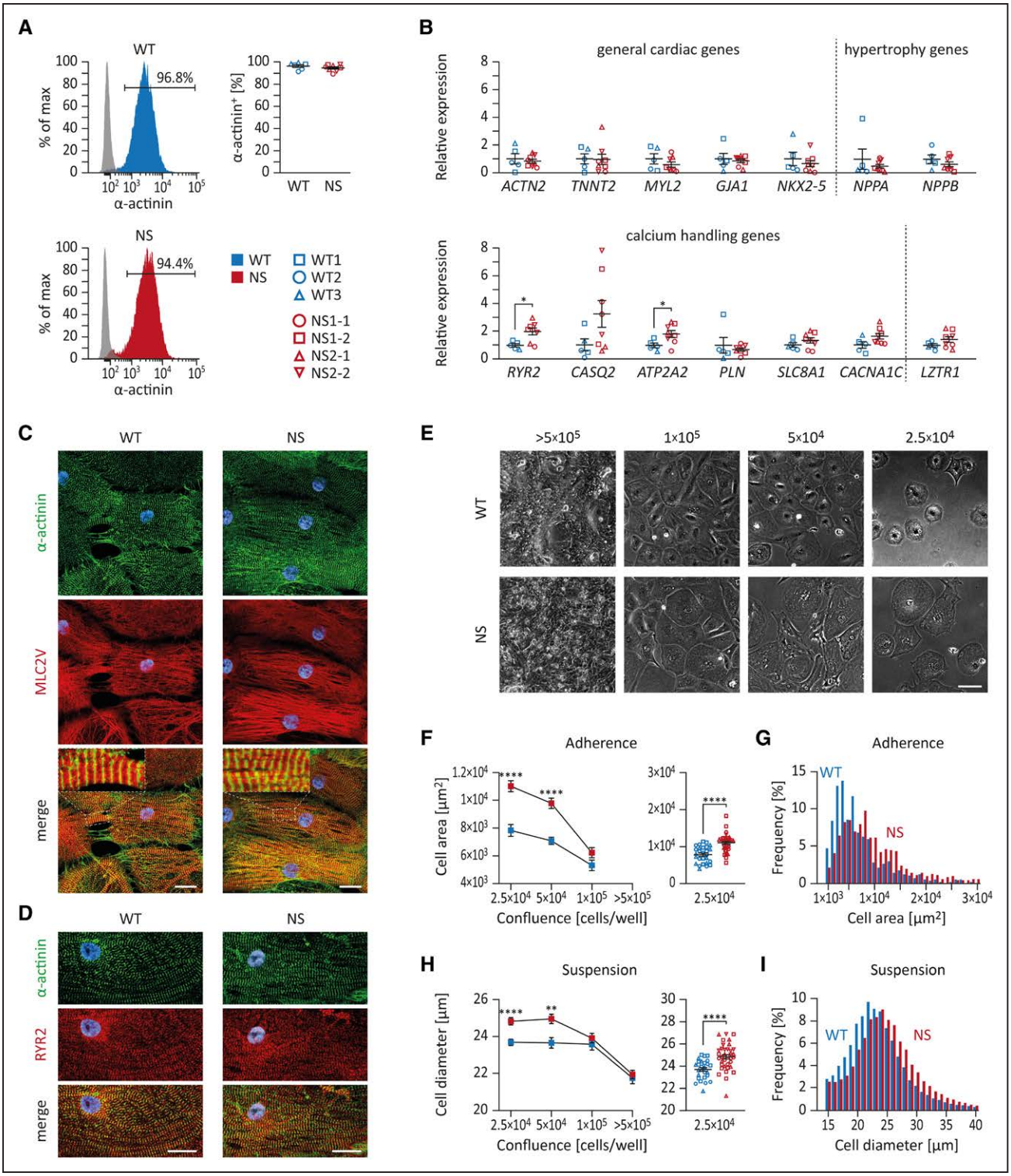

Figure 2. Patient-specific cardiomyocytes recapitulate the hypertrophic disease phenotype.
A, Flow cytometry analysis of iPSC-CMs for α-actinin at day 27 to 35 of cardiac differentiation. Representative measurements (iPSC lines WT1 and NS1-2) and quantitative analysis displayed robust differentiation efficiencies (for WT: n=6 independent differentiations, 3 iPSC lines; for NS: n=8 independent differentiations, 4 iPSC lines, 2 per patient). Gray peaks represent the isotype controls. **B**, Expression of cardiac-specific genes was assessed by real-time polymerase chain reaction analysis in WT and NS iPSC-CMs at day 60 to 75 (for WT: n=5 independent differentiations, 3 iPSC lines; for NS: n=8 independent differentiations, 4 iPSC lines, 2 per patient). Samples were analyzed in triplicates and data were normalized to *GAPDH* and *ACTB* expression and WT controls. **C** and **D**, Structural characterization of WT and NS iPSC-CMs at day 85 to 88 via immunofluorescence staining for ventricular-specific MLC2V (red) and α-actinin (green) and for sarcoplasmic reticulum calcium channel RYR2 (red) displayed well-organized sarcomeric organization. Shown are representative images (iPSC line WT2 and NS2-2). Nuclei were costained with 4′,6-diamidino-2-phenylindole (blue). Scale bar, 20 µm. **E** through **I**, Cell size measurements were obtained from WT and NS iPSC-CM cultures between days 60 to 84, plated at various densities to determine the size distribution in correlation to cell confluence. **E**, Representative images of the iPSC-CM cultures (iPSC line WT3 and NS2-1). Scale bar, 100 µm. **F**, Quantification of cell area in adherent cultures of WT and NS iPSC-CMs, assessed by manual size measurements, (*Continued*)

Figure 2 Continued. revealed a significant increase in cell area in NS cultures compared with WT controls at lower plating densities (for WT: n=27 samples, 9 independent differentiations, 3 iPSC lines; for NS: n=36 samples, 12 independent differentiations, 4 iPSC lines, 2 per patient). **G**, Corresponding cell size distribution of adherent cultures at confluency of 2.5×10^4 cells per well. **H**, Quantitative analysis of cell diameter in suspension in singularized iPSC-CM cultures, assessed by CASY cell counter, displayed a hypertrophic cell diameter in NS cells compared with WT at lower confluency (for WT: n=27 samples, 9 independent differentiations, 3 iPSC lines; for NS: n=36 samples, 12 independent differentiations, 4 iPSC lines, 2 per patient). **I**, Corresponding cell size distribution of suspension cultures at confluency of 2.5×10^4 cells per well. Data are presented as mean±SEM. *P<0.05, **P<0.01, ****P<0.0001 by nonparametric Mann-Whitney test (**A**, **B**, **F**, and **H**). iPSC-CM indicates induced pluripotent stem cell–derived cardiomyocytes; NS, Noonan syndrome; and WT, wild type.

by a fine balance of calcium and potassium fluxes via the sarcolemma, was reduced in NS when compared with healthy donors (Figure 3M). No differences were observed in the resting membrane potential, AP amplitude, maximum depolarization velocity and AP duration at 90% repolarization between patients' and control cells (Figure 3J through 3L and 3N).

Next, we investigated calcium transients (CaTs) and cytosolic calcium sparks in patient-specific iPSC-CMs using confocal line scan imaging. Analysis of CaTs under basal conditions revealed that iPSC-CMs from the NS patients exhibited a significantly faster CaT rise time and a shorter duration of CaTs at 50% decay compared with WT iPSC-CMs (Figure 4A through 4C). Besides alterations in CaTs, significant changes in spontaneous diastolic calcium release from the sarcoplasmic reticulum (SR) in the patients' cells were observed (Figure 4D). NS iPSC-CMs exhibited a higher calcium spark frequency compared with control iPSC-CMs (Figure 4E). The calculated overall diastolic SR calcium leak was 3-fold higher in NS iPSC-CMs compared with WT cells (Figure 4F). These data, in conjunction with the identification of the dysregulation of calcium handling genes (Figure 2B), suggest a calcium handling imbalance in the NS iPSC-CMs. Given the hypertrophy- and arrhythmia-inducing effects of elevated calcium, we reasoned that the administration of a calcium channel blocker, in line with recent clinical recommendations[41] and observations from earlier studies in iPSC models of HCM,[42–44] may be of therapeutic value in the described NS patient model. Indeed, verapamil at a therapeutic concentration of 100 nmol/L[45] prolonged the CaT rise time and increased the duration of CaT decay in the NS iPSC-CMs (Figure 4B and 4C). Further, the diastolic SR calcium leak was normalized in the patients' cells (Figure 4E and 4F).

In summary, our data support the use of calcium channel blockers such as verapamil in the treatment of NS-related dysregulation of calcium homeostasis in consequence of *LTZR1* loss-of-function mutations.

LZTR1-Deficient Cardiomyocytes Demonstrate Enhanced RAS-MAPK Signaling

To decipher the underlying molecular mechanisms contributing to the severe left ventricular hypertrophy in the identified NS patients, we performed transcriptome and proteome analyses in the *LZTR1*-deficient and WT iPSC-CM cultures. As anticipated, transcriptome data obtained by RNA sequencing clustered according to their respective genotypes (Figure 5A). We found 444 significantly upregulated and 777 significantly downregulated candidates in the *LZTR1*-deficient NS cells (Figure 5B; the top 100 differentially expressed genes are presented in Figure IV in the Data Supplement). Kyoto Encyclopedia of Genes and Genomes (KEGG) pathway analysis of differentially expressed genes indicated that target genes were enriched in multiple cardiac-related biological processes (such as extracellular matrix-receptor interaction, HCM, regulation of the actin cytoskeleton, and calcium signaling), as well as in the PI3K-Akt and the RAS-MAPK signaling—two major pathways that directly involve RAS proteins (Figure 5C, Figure V in the Data Supplement). Quantitative proteomics based on spike-in stable isotope labeling by amino acids in cell culture (SILAC; Figure 5D)[36,46] identified 283 proteins as differentially regulated between NS and WT iPSC-CMs. In agreement with the transcriptome data, we identified enhanced abundance of RAS isoform NRAS, HRAS and especially muscle RAS oncogene homolog (MRAS) in the *LZTR1*-deficient CMs (Figure 5E and 5F). These findings were confirmed by Western blot analyses for pan-RAS (recognizing all RAS isoforms) and the critical RAS-MAPK downstream signaling proteins p44/p42 MAPK (ERK1 and ERK2) in the *LZTR1*-deficient NS iPSC-CMs (Figure 5G and 5H); note that no suitable antibody for the detection of endogenous LZTR1 in our cell model could be identified or generated. Significantly elevated levels of RAS proteins were detected in *LZTR1*-deficient NS cultures, in line with an LZTR1-cullin 3 ubiquitin ligase complex-mediated RAS protein degradation in human CMs (Figure 5G and 5I). The protein expression of phosphorylated ERK was also significantly increased in the *LZTR1*-deficient NS compared with WT cells (Figure 5G and 5J through 5L). In contrast to the RAS-MAPK hyperactivity, the PI3K-Akt signaling appears to be unaffected in the *LZTR1*-deficient NS cultures (Figure 5G and 5M through 5O).

These data clearly point toward an accumulation of RAS proteins in the *LZTR1*-deficient NS iPSC-CMs, resulting in enhanced RAS-MAPK signaling commonly observed in NS and other RASopathies.

Drug Treatment of Patient-Specific Cardiomyocytes Does Not Attenuate Cardiac Hypertrophy

We further tested whether pharmacological intervention with verapamil or MEK inhibitor U0126 may

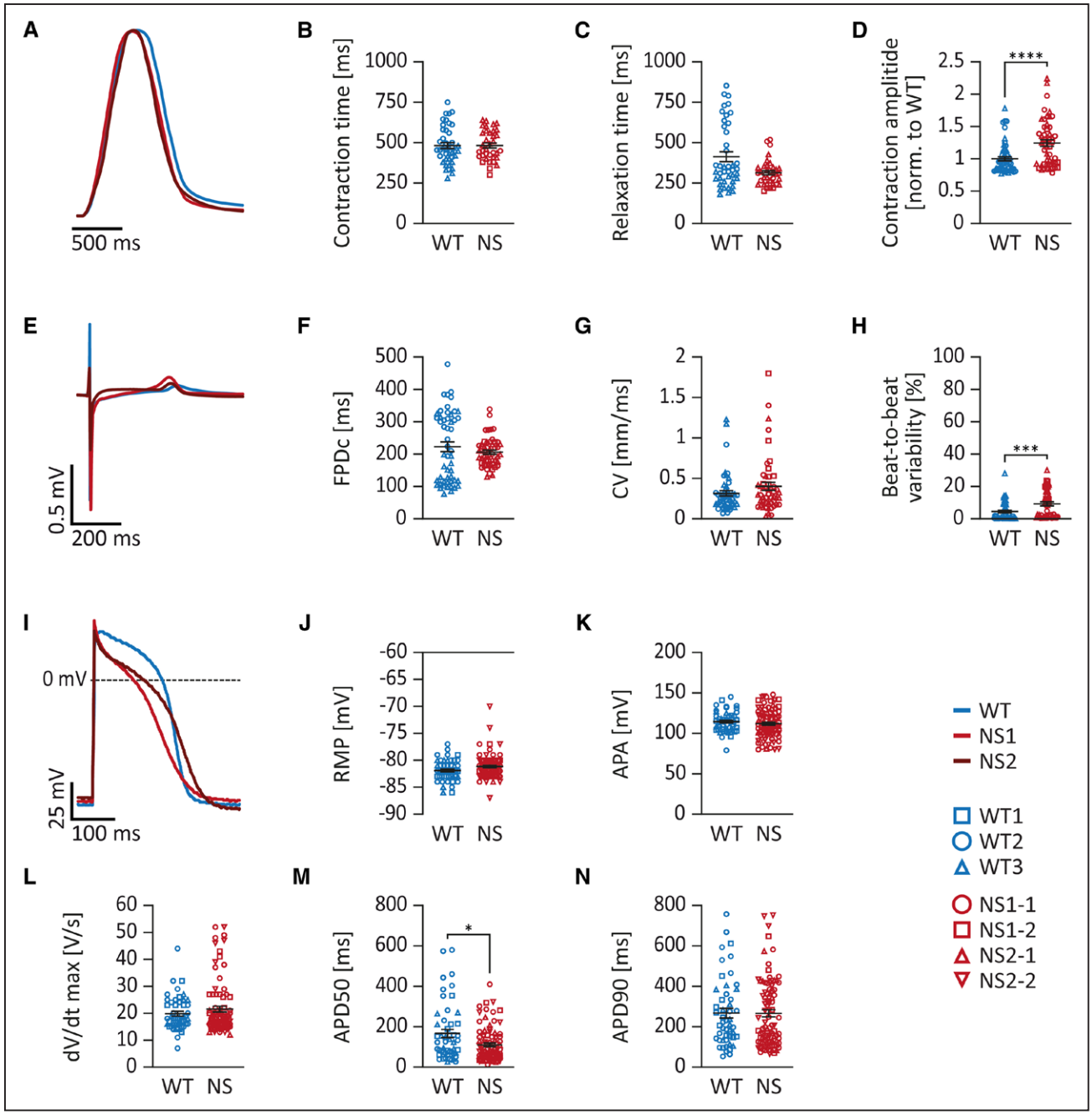

Figure 3. Patient-specific cardiomyocytes mostly feature regular contractile function and electrophysiology.
A through **C**, Contractility in spontaneously contracting iPSC-CM cultures at day 49 to 72 was assessed by video recordings (for WT: n=42 samples, 8 independent differentiations, 2 iPSC lines; for NS: n=36 samples, 8 independent differentiations, 3 iPSC lines, 1 to 2 per patient). **A**, Representative normalized contraction curves (iPSC lines WT2, NS1-1 and NS2-1), and quantitative analysis of (**B**) contraction time and (**C**) relaxation time to 50% decay of the curve. **D** through **H**, Contraction and field potential parameters of iPSC-CM cultures at day 53 to 76 were analyzed using a multielectrode array. **D**, Analysis of contraction amplitude as change of impedance (for WT: n=55 samples, 7 independent differentiations, 2 iPSC lines; for NS: n=51 samples, 8 independent differentiations, 3 iPSC lines, 1 to 2 per patient). **E**, Representative traces of field potential (iPSC lines WT2, NS1-1 and NS2-1), and quantitative analysis of (**F**) corrected field potential duration (FPDc; normalized to beat rate using the Fridericia correction formula), (**G**) conduction velocity, and (**H**) beat-to-beat variability (for WT: n=52 samples, 7 independent differentiations, 2 iPSC lines; for NS: n=51 samples, 9 independent differentiations, 3 iPSC lines, 1 to 2 per patient). **I** through **N**, AP parameters of iPSC-CMs at days 60 to 76, stimulated at 1 Hz, were assessed by whole-cell patch-clamp recordings (for WT: n=50 cells, 5 independent differentiations, 3 iPSC lines; for NS: n=89 cells, 7 independent differentiations, 4 iPSC lines, 2 per patient). **I**, Representative traces of APs (iPSC lines WT2, NS1-1 and NS2-2), and quantitative analysis of (**J**) RMP, (**K**) APA, (**L**) dV/dt max, (**M**) APD50, and (**N**) APD90. Data are presented as mean±SEM. **P*<0.05, ****P*<0.001, *****P*<0.0001 by nonparametric Mann-Whitney test (**B** through **D**, **F** through **H**, **J** through **N**). AP indicates action potential; APA, action potential amplitude; APD50, action potential duration at 50% repolarization; APD90, action potential duration at 90% repolarization; CV, conduction velocity; dV/dt max, maximal depolarization velocity; FPDc, corrected field potential duration; iPSC-CM, induced pluripotent stem cell–derived cardiomyocytes; NS, Noonan syndrome; RMP, resting membrane potential; and WT, wild type.

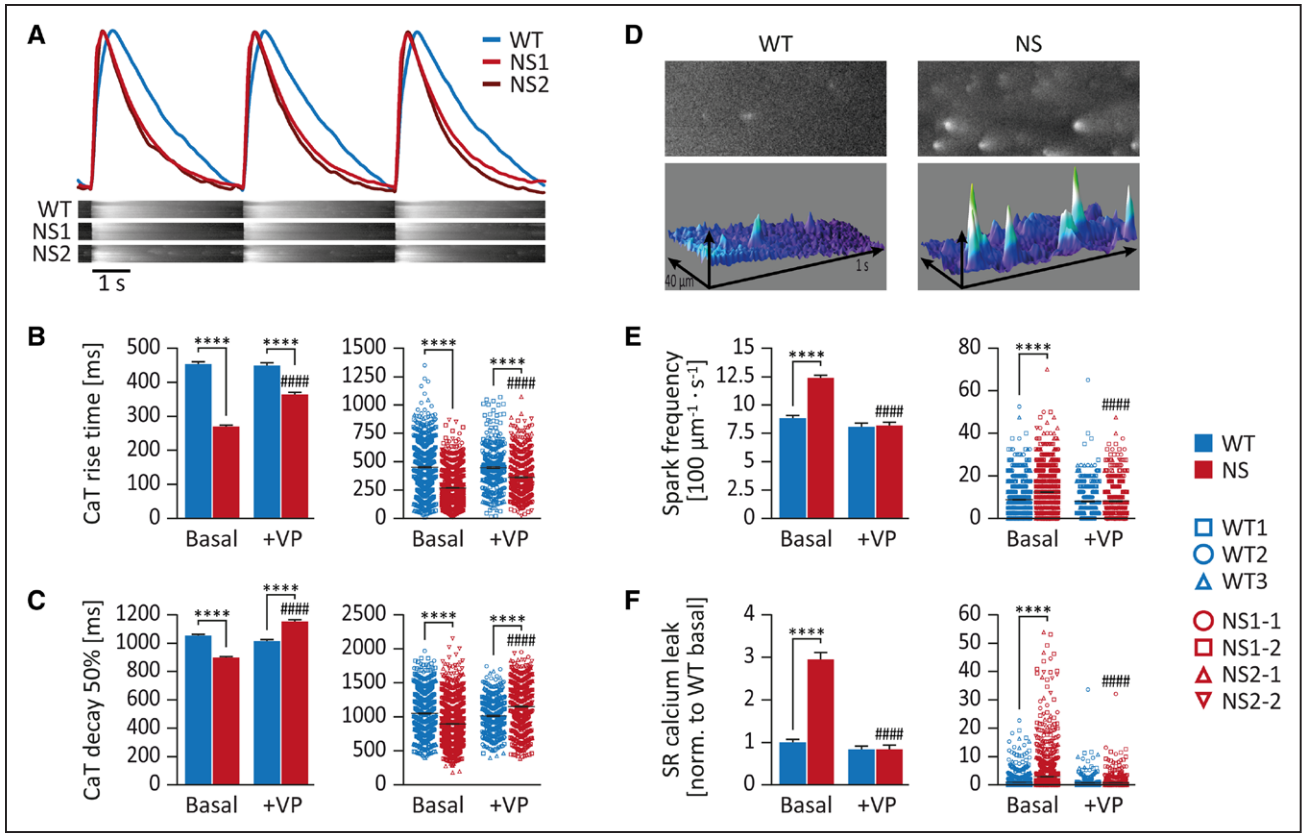

Figure 4. Patient-specific cardiomyocytes display altered calcium homeostasis.
For calcium recordings, iPSC-CMs at days 56 to 76 were loaded with calcium indicator Fluo-4 AM, paced at 0.25 Hz and analyzed via confocal imaging under basal conditions and after treatment with 100 nmol/L VP (for WT: n=490–1000 cells, 11 independent differentiations, 3 iPSC lines; for NS: n=698–1470 cells, 18 independent differentiations, 4 iPSC lines, 2 per patient). **A**, Representative plots of calcium transients (CaTs) with the corresponding recordings below (iPSC line WT2, NS1-2 and NS2-1), and quantitative analysis of (**B**) CaT rise time and (**C**) CaT decay at 50%. **D**, Representative plots of diastolic calcium sparks in WT iPSC-CMs and NS iPSC-CMs with the corresponding 3D surface plots below (iPSC line WT2 and NS1-1) and quantitative analysis of (**E**) spark frequency and (**F**) overall diastolic calcium leak. Data are presented as mean±SEM. ****/####P<0.0001 by nonparametric Kruskal-Wallis test with Dunn correction (**B**, **C**, **E**, and **F**). * indicates significance to WT, # indicates significance to basal condition. iPSC-CM indicates induced pluripotent stem cell–derived cardiomyocytes; NS, Noonan syndrome; VP, verapamil; and WT, wild type.

prevent the pathological hypertrophy in NS iPSC-CMs. First, we verified that the drug doses applied (verapamil at 100 nmol/L, U0126 at 10 µmol/L) had no influence on cell viability (Figure 6A through 6D). Long-term treatment with verapamil or U0126 for 20 days resulted in slightly reduced, but not fully normalized CM sizes in NS (Figure 6E and 6F). U0126 dramatically inhibited RAS-MAPK signaling, whereas verapamil did not show any significant impact on signaling activity after 20 days of intervention (Figure 6G through 6K).

Summarizing, drug treatment with calcium channel blockers or MEK inhibitors did not significantly attenuate cellular hypertrophy in *LZTR1*-deficient NS iPSC-CMs.

Intronic CRISPR Repair in Patient-Specific Cardiomyocytes Rescues the Disease Phenotype

In an attempt to rescue the phenotype and provide proof-of-concept for a sustainable therapeutic approach, we explored CRISPR/Cas9-based genome editing aiming at the disruption of the SNP-induced donor splice site in the paternal allele. We reasoned that this approach would reintroduce regular translation from the paternal allele, and thereby mimic the maternal genotype with no clinical phenotype despite *LTZR1* haploinsufficiency caused by the maternal exon 1 premature stop codon. We tested 2 genome editing approaches: (1) targeted disruption of the paternal *LZTR1* intron 16 mutation by simple CRISPR/Cas9-mediated nonhomologous end joining; and (2) a CRISPR/Cas9 approach with a pair of guide RNAs for removal of a ≈71 bps short fragment surrounding the intronic mutation (Figure 7A). As anticipated, targeting of the paternal allele by CRISPR/Cas9 resulted in variable indels. All of the observed variants, except for 1 (insertion of a T), are predicted to result in the destruction of the SNP-induced donor splice site (Figure VI in the Data Supplement). We finally investigated 2 edited iPSC lines with different intronic deletions for each NS iPSC model (NS1: –71 bps and –9 bps deletions; NS2: –2 bps and –9 bps deletions) to scrutinize whether the pathological hypertrophy phenotype could be reversed (Figure 7B,

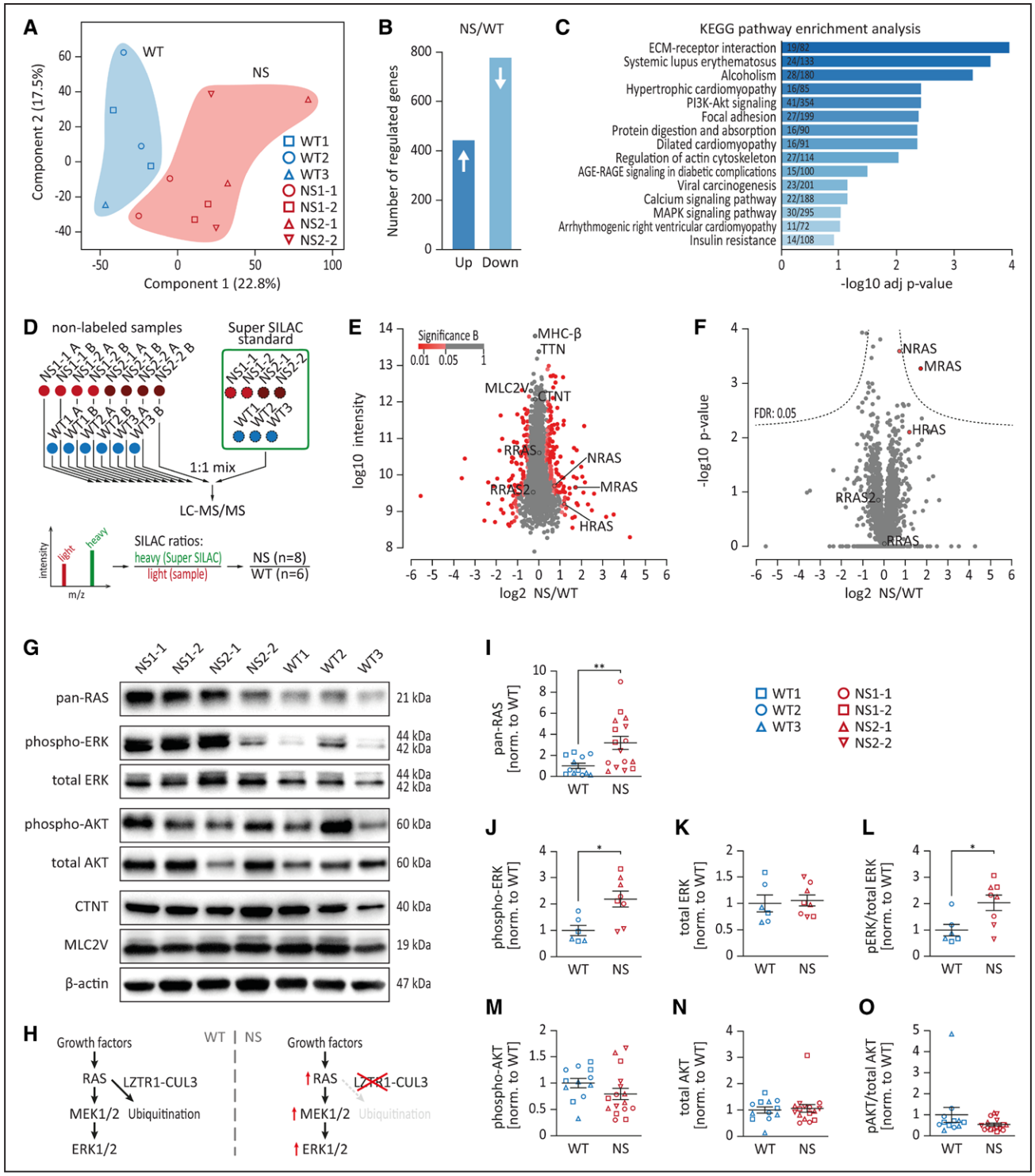

Figure 5. LZTR1-deficient cardiomyocytes demonstrate enhanced RAS-MAPK signaling.

A through **C**, Transcriptomic analysis of iPSC-CMs at days 60 to 75 by RNA sequencing (for WT: n=5 independent differentiations, 3 iPSC lines; for NS: n=8 independent differentiations, 4 iPSC lines, 2 per patient). **A**, Principle component analysis of the entire gene set of NS cultures and WT controls revealed a clustering according to disease vs no disease. **B**, Numbers of up- and downregulated genes in NS compared with WT samples. The top 100 significantly regulated genes are presented in Figure IV in the Data Supplement. **C**, Kyoto Encyclopedia of Genes and Genomes (KEGG) pathway enrichment analysis of biological processes. Numbers represent enriched genes of total genes. **D** through **F**, Quantitative proteomics of iPSC-CMs at days 68 to 71 using spike-in super-SILAC (spike-in stable isotope labeling by amino acids in cell culture) standard (for WT: n=6 independent differentiations, 3 iPSC lines; for NS: n=8 independent differentiations, 4 iPSC lines, 2 per patient). **D**, Depiction of labeling and analysis process: Pooled samples of NS and WT iPSC-CM cultures labeled with "heavy" amino acids were used as spike-in super-SILAC standard; nonlabeled samples were mixed 1:1 with the standard; peptide fold–change ratios of the individual "light" samples were calculated and the overall ratio between NS and WT was determined. **E**, Depiction of the relative abundance of 2440 proteins between NS and WT iPSC-CMs. Two hundred eighty-three proteins with significantly different abundance between NS and WT samples are highlighted in red. **F**, Volcano plot of detected proteins with RAS isoforms highlighted. **G** through **O**, Analysis of RAS-MAPK signaling activity in unstimulated WT and NS iPSC-CMs at days 60 to 81, (*Continued*)

Figure 5 Continued. assessed by Western blot. **G**, Representative images of signaling activity analysis for RAS, phosphorylated ERK (Thr202/Tyr204 of p44 MAPK and Thr185/Tyr187 of p42 MAPK), total ERK, phosphorylated AKT (Ser473), and total AKT. Expression of cardiac troponin T (CTNT), ventricular-specific MLC2V and housekeeping protein β-actin indicated comparable amounts of iPSC-CMs in the samples. **H**, Model of LZTR1-mediated regulation of RAS-MAPK signaling in WT and NS. Quantitative analyses of (**I**) pan-RAS, (**J**) phosphorylated ERK, (**K**) total ERK, (**L**) overall ratio of phosphorylated to total ERK expression, (**M**) phosphorylated AKT, (**N**) total AKT, and (**O**) overall ratio of phosphorylated to total AKT expression revealed elevation of the RAS-MAPK signaling, but not of the PI3K-Akt pathway in the patients' iPSC-CMs. Data were normalized to total protein and WT controls (for WT: n=6–12 independent differentiations, 3 iPSC lines; for NS: n=8–16 independent differentiations, 4 iPSC lines, 2 per patient). Data are presented as mean±SEM. **P*<0.05, ***P*<0.01 by nonparametric Mann-Whitney test (**I** through **O**). AGE-RAGE indicates advanced glycation endproducts/receptor for advanced glycation endproducts; ECM, extracellular matrix; FDR, false discovery rate; iPSC-CM, induced pluripotent stem cell–derived cardiomyocytes; MAPK, mitogen-activated protein kinase; NS, Noonan syndrome; and WT, wild type.

and Figure VII in the Data Supplement). Analysis of the *LZTR1* transcript confirmed the loss of the cryptic exon within the paternal allele in the edited NS iPSC lines (Figure 7C). Cardiac differentiation efficiency and sarcomeric organization were similarly high in the corrected and uncorrected iPSC-CMs (Figure 7D and 7E). In line with our "therapeutic" goal, we observed a largely normalized cell size in the corrected iPSC-CMs from both patients (Figure 7F and 7G). The contractile and electrophysiological properties of the corrected CMs were comparable with WT (Figure 7H through 7M).

Collectively, these data support our hypothesis that CRISPR/Cas9-mediated destruction of the intronic donor splice site can reverse the NS-associated hypertrophic phenotype in CMs.

Intronic CRISPR Repair Normalizes the Disease-Specific Proteome Signature

To further clarify whether the phenotypic changes are the result of the normalization of RAS-MAPK signaling, we first subjected the CRISPR-corrected iPSC-CMs to SILAC-based proteomics using a similar experimental strategy as outlined above (Figure 8A). Indeed, RAS isoforms—including MRAS, NRAS, and KRAS—were not found to be elevated in the edited NS iPSC-CMs (Figure 8B). Western blot analyses verified this finding and confirmed a normalization of RAS-MAPK signaling activity to WT control levels (Figure 8C through 8G). To further specify the disease-specific protein signature and identify potential candidates for pharmacological interventions, we compared the differentially expressed proteins of the NS versus WT iPSC-CMs (Figure 5E) with the differentially expressed proteins of the corrected versus noncorrected cultures (Figure 8H and 8I). This analysis confirmed 85 proteins as disease-specific candidates in NS (Figure 8H). A subset of proteins of the overlapping profile, such as MRAS,[47,48] ubiquitin-like molecule interferon-stimulated gene 15 (ISG15),[49,50] ubiquitin carboxyl-terminal hydrolase 15 (USP15),[51] and annexin A1 (ANXA1),[52,53] are linked to the regulation of the RAS-MAPK pathway. Furthermore, multiple proteins that are involved in cardiac hypertrophy and calcium signaling, such as the calcium/calmodulin-dependent protein kinase II (CAMK2A),[54,55] calcium-shuttle protein sarcalumenin (SRL),[56,57] glucose transporter protein type 1 (SLC2A1),[58,59] adenylosuccinate synthetase 1 (ADSS1),[60] and aldolase A (ALDOA),[61] demonstrated a significantly higher abundance in *LZTR1*-deficient iPSC-CMs and were normalized after intronic CRISPR repair. The complementary RNA sequencing profile of the CRISPR-corrected iPSC-CMs is presented in Figure VIII in the Data Supplement.

Taken together, these data verified the *LZTR1* variants to be causative in the development of the cardiac hypertrophy, uncovered a disease-specific proteome signature for *LZTR1*-associated NS (Figure 8I) and revealed that the intronic CRISPR repair of the paternal *LZTR1* allele could be considered as a treatment option in the 2 index patients with NS.

DISCUSSION

After clinical suspicion of an NS spectrum disorder with severe HCM and exclusion of mutations in typically NS-associated genes, we performed whole-exome sequencing on the affected siblings. This revealed distinct biallelic mutations in *LZTR1*, both causing early protein truncation and leading to complete or partial loss-of-function. Our finding highlights the necessity to additionally screen whole-exome sequencing data sets for deep-intronic regions and putative novel splice sites.[62,63] Recently, Biesecker et al described 12 families with mutations in *LZTR1*, providing substantial genetic evidence that autosomal recessive mutations in *LZTR1* are associated with a clinical spectrum of symptoms resembling NS.[23] In addition to the clinical diagnosis, we now provide evidence that the RAS-MAPK pathway is in fact activated, confirming the RASopathy hypothesis in patients with NS and *LZTR1* loss-of-function. Given that both patients presented with a very early onset of HCM—in 1 of the cases even documented as prenatal onset—we suggest that beside mutations in *RAF1* and *RIT1*,[10–12] *LZTR1* loss-of-function mutations confer a high risk for the development of HCM. Our findings have important implications for genetic counseling, molecular diagnostic strategies (autosomal dominant versus autosomal recessive *LZTR1* mutations) as well as clinical management of patients. Moreover, it is of great clinical relevance to understand the underlying molecular and functional mechanisms leading to the severe cardiac phenotype in *LZTR1*-associated NS and to identify novel therapeutic targets for a more precise and more effective treatment.

To model the *LZTR1*-associated NS in vitro and to obtain novel insights into the pathomechanisms, we utilized the versatile iPSC approach to generate

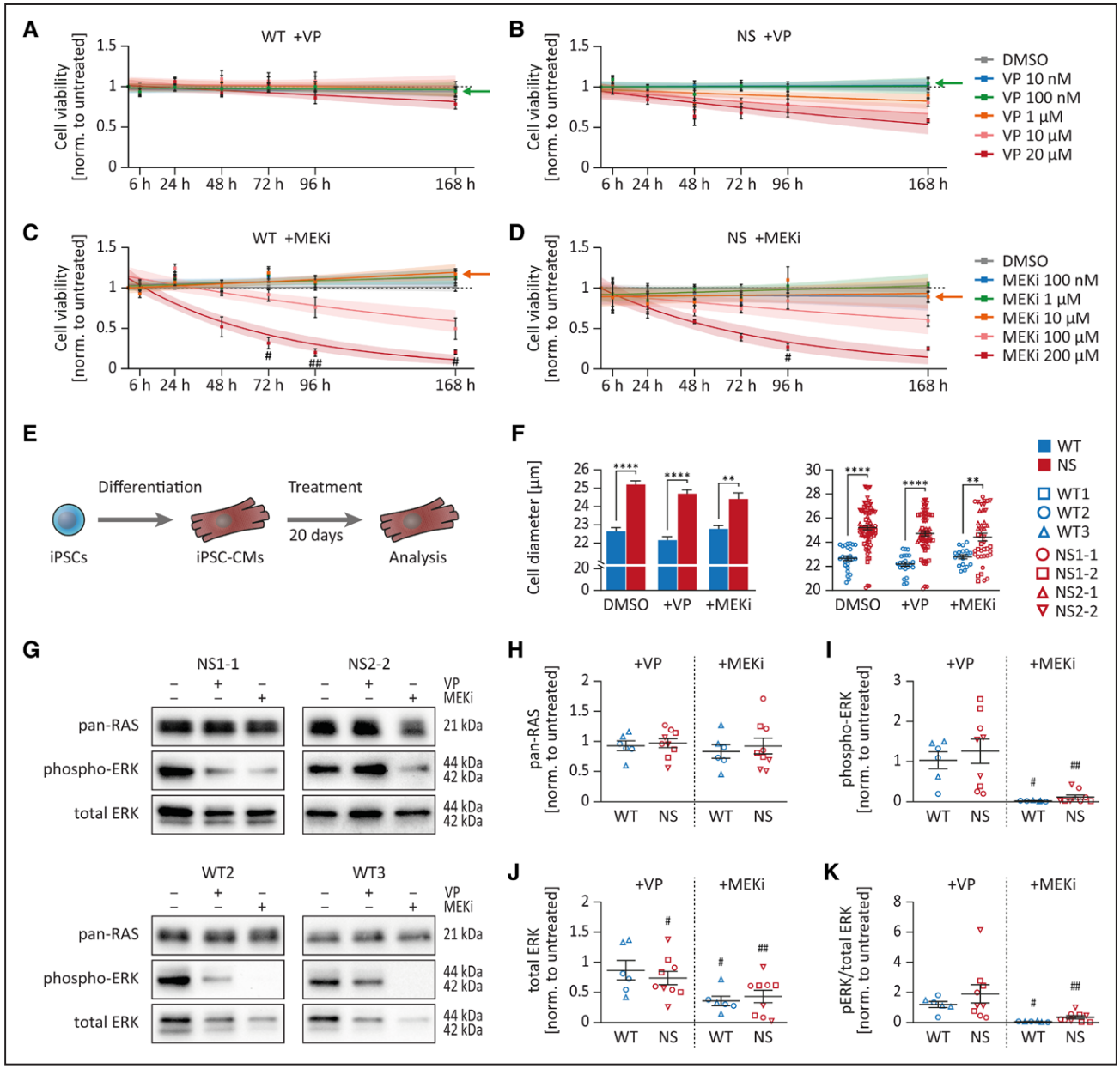

Figure 6. Drug treatment of patient-specific cardiomyocytes does not attenuate cardiac hypertrophy.
A to **D**, Analysis of cell viability on treatment with different drugs (for WT: n=9 samples per concentration, 3 independent differentiations, 2 iPSC lines; for NS: n=6 samples per concentration, 2 independent differentiations, 2 iPSC lines, 1 per patient). WT and NS iPSC-CMs at days 70 to 89 were treated with different concentrations of (**A** and **B**) calcium channel blocker VP and (**C** and **D**) MEK inhibitor U0126 (MEKi) for 7 days. Both drugs do not decrease cell viability at the concentrations used for long-term treatment (arrows). **E** through **K**, Cultures of iPSC-CMs were analyzed for cell size and RAS-MAPK activity after long-term treatment with 100 nmol/L VP or 10 µmol/L MEKi for 20 days. **E**, Schematic protocol of the treatment. **F**, Quantitative analysis of cell diameter in suspension in VP- and MEKi-treated iPSC-CM cultures, plated at single cell level with 2.5×10^4 cells per well and assessed by CASY cell counter at days 53 to 88 (for WT2: n=18–27 samples, 8 independent differentiations; for NS: n=42–81 samples, 23 independent differentiations, 4 iPSC lines, 2 per patient). **G** through **K**, Analysis of RAS-MAPK signaling activity in VP- and MEKi-treated iPSC-CMs at days 61 to 69, assessed by Western blot for RAS, phosphorylated ERK (Thr202/Tyr204 of p44 MAPK and Thr185/Tyr187 of p42 MAPK), and total ERK. Shown are (**G**) representative images and quantitative analysis of (**H**) pan-RAS, (**I**) phosphorylated ERK, (**J**) total ERK, and (**K**) overall ratio of phosphorylated to total ERK protein expression. Data were normalized to total protein and corresponding untreated samples (for WT: n=6 independent differentiations, 2 iPSC lines; for NS: n=9 independent differentiations, 3 iPSC lines, 1–2 per patient). Data are presented as mean±SEM. $^{\#}P<0.05$, $^{**}/^{\#\#}P<0.01$, $^{****}P<0.0001$ by nonparametric Kruskal-Wallis test with Dunn correction (**A** through **D**, **F**), or by nonparametric 1-sample Wilcoxon test (**H** through **K**). * indicates significance to WT, # indicates significance to untreated condition. DMSO indicates dimethylsulfoxide; iPSC-CM, induced pluripotent stem cell–derived cardiomyocytes; MAPK, mitogen-activated protein kinase; NS, Noonan syndrome; VP, verapamil; and WT, wild type.

patient-specific functional CMs. We found that (1) the patient-specific iPSC-CMs recapitulate the hypertrophic phenotype with evidence of abnormal calcium handling as a contributor to the clinical NS disease phenotype; (2) L-type calcium channel blockade and MEK inhibition resulted in a normalization of calcium homeostasis and RAS-MAPK signaling activity, respectively, providing a molecular underpinning for the clinical use of these

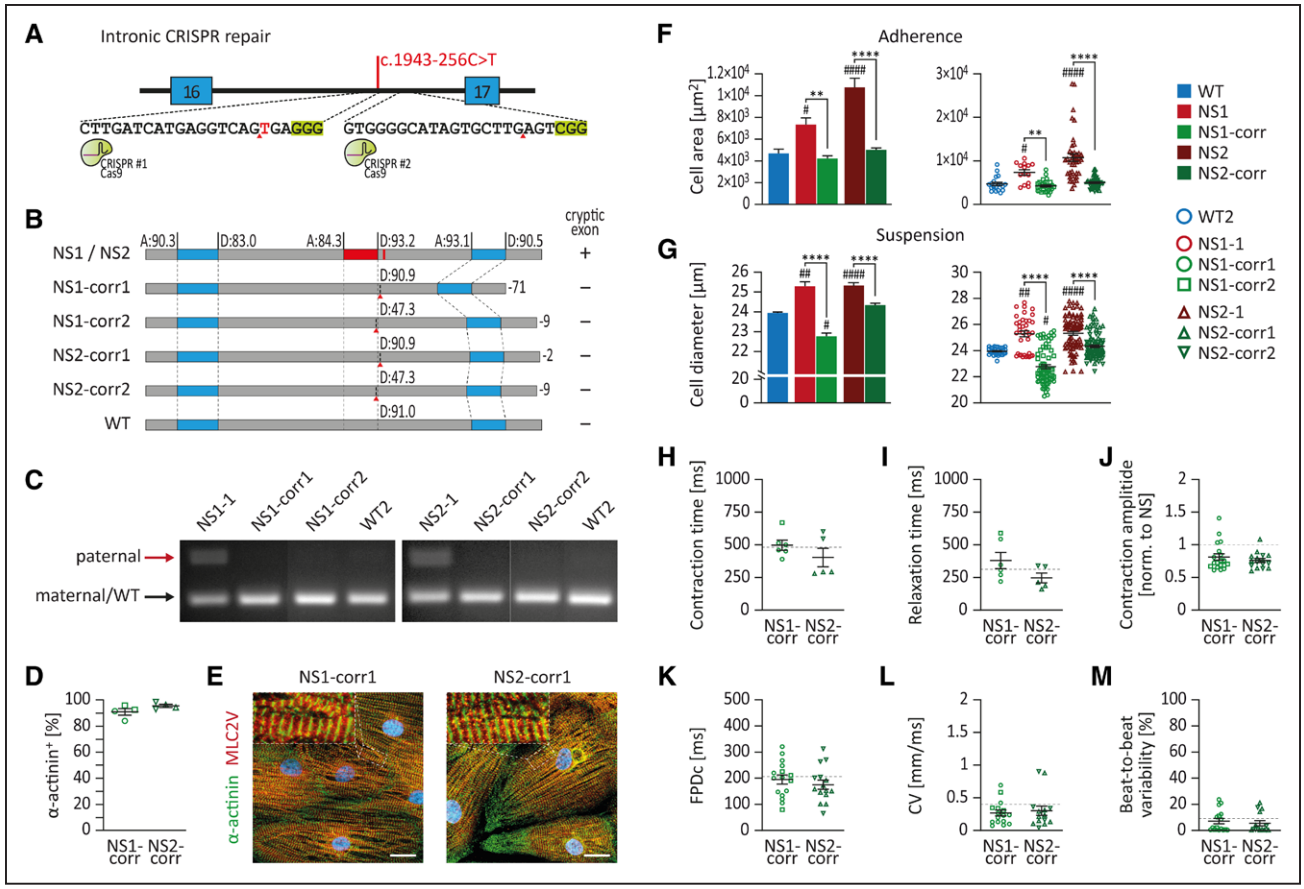

Figure 7. Intronic CRISPR repair in patient-specific cardiomyocytes rescues the disease phenotype.
A, Depiction of CRISPR/Cas9 genome editing approach: Either 1 or 2 allele-specific CRISPR guide RNAs were applied to delete a fragment flanking the intronic mutation in *LZTR1* on the paternal allele. **B**, Two CRISPR-repaired clones per index patient with different indels, exclusively occurring on the paternal allele, were selected. Prediction of donor ("D") and acceptor ("A") splice sites between exons 16 and 17 in corrected iPSC lines showed reduced probability for the disease-causing splicing event within intron 16. **C**, The additional cryptic exon in the patients' iPSCs was not detectable in *LZTR1* transcripts of all 4 corrected iPSC lines, assessed by reverse transcriptase polymerase chain reaction of exons 16 to 17. **D**, Flow cytometry analysis for α-actinin at days 27 to 39 of cardiac differentiation (for NS1-corr: n=4 independent differentiations, 2 iPSC lines; for NS2-corr: n=4 independent differentiations, 2 iPSC lines). **E**, Representative immunofluorescence stainings of corrected iPSC-CMs at days 61 to 65 (iPSC line NS1-corr1 and NS2-corr1) for ventricular-specific MLC2V (red) and α-actinin (green). Nuclei were costained with 4′,6-diamidino-2-phenylindole (blue). Scale bar, 20 µm. **F** and **G**, Cell size analysis from WT, NS, and corrected iPSC-CMs, plated at 2.5×10^4 cells per well with measurements acquired between days 60 to 84, revealed a significant decrease of cell size to WT levels in corrected compared with diseased iPSC-CMs. **F**, Quantification of cell area in adherent cultures (for WT2: n=19 samples, 6 independent differentiations; for NS1-1: n=14 samples, 3 independent differentiations; for NS1-corr: n=29 samples, 6 independent differentiations, 2 iPSC lines; for NS2-1: n=42 samples, 7 independent differentiations; for NS2-corr: n=45 samples, 8 independent differentiations, 2 iPSC lines) and (**G**) CASY cell counter analysis of cell diameter in suspension in singularized iPSC-CMs (for WT2: n=36 samples, 3 independent differentiations; for NS1-1: n=36 samples, 3 independent differentiations; for NS1-corr: n=72 samples, 6 independent differentiations, 2 iPSC lines; for NS2-1: n=84 samples, 7 independent differentiations; for NS2-corr: n=91 samples, 8 independent differentiations, 2 iPSC lines). **H** and **I**, Contractility in spontaneously contracting iPSC-CM cultures at days 43 to 67 was assessed by video recordings (for NS1-corr: n=6 samples, 4 independent differentiations, 2 iPSC lines; for NS2-corr: n=5 samples, 3 independent differentiations, 2 iPSC lines). Analysis of (**H**) contraction time and (**I**) relaxation time to 50% decay of the curve. **J** through **M**, Contraction and field potential parameters of iPSC-CM cultures at days 48 to 74 were analyzed using a multielectrode array. Analysis of (**J**) contraction amplitude by impedance change (for NS1-corr: n=19 samples, 7 independent differentiations, 2 iPSC lines; for NS2-corr: n=16 samples, 7 independent differentiation experiments, 2 iPSC lines). Analysis of (**K**) FPDc, normalized to beat rate using the Fridericia correction formula, (**L**) conduction velocity, and (**M**) beat-to-beat variability (for NS1-corr: n=16 samples, 6 independent differentiations, 2 iPSC lines; for NS2-corr: n=15 samples, 6 independent differentiations, 2 iPSC lines). Dashed lines represent mean values in NS (see Figure 3). Data are presented as mean±SEM. $^{\#}P<0.05$, $^{**/\#\#}P<0.01$, $^{****/\#\#\#\#}P<0.0001$ by nonparametric Mann-Whitney test (**D**, **H** through **M**) or by nonparametric Kruskal-Wallis test with Dunn correction (**F** and **G**). * indicates significance to respective NS cell line, # indicates significance to WT. CV indicates conduction velocity; FPDc, corrected field potential duration; iPSC-CM, induced pluripotent stem cell–derived cardiomyocytes; NS, Noonan syndrome; and WT, wild type.

drugs in patients with NS; and (3) destruction of the mutation-induced donor splice site in iPSCs from the identified index patients may serve as a means for therapeutic genome editing.

The pronounced hypertrophy with the associated risk for developing arrhythmias was the major issue in our index patients. Therefore, a first focus was given on the analysis of the hypertrophic phenotype and on the electrophysiological and calcium handling properties in the patient-specific iPSC-CMs. Investigating 4 NS iPSC lines, 2 of each index patient, and 3 independent healthy controls, we found that the patients' iPSC-CMs displayed a significantly enlarged cell size. Interestingly, no obvious disarray of sarcomeres was detected in our cell model, which clearly distinguished it from previous iPSC-CM models of both NS-associated HCM[28] and

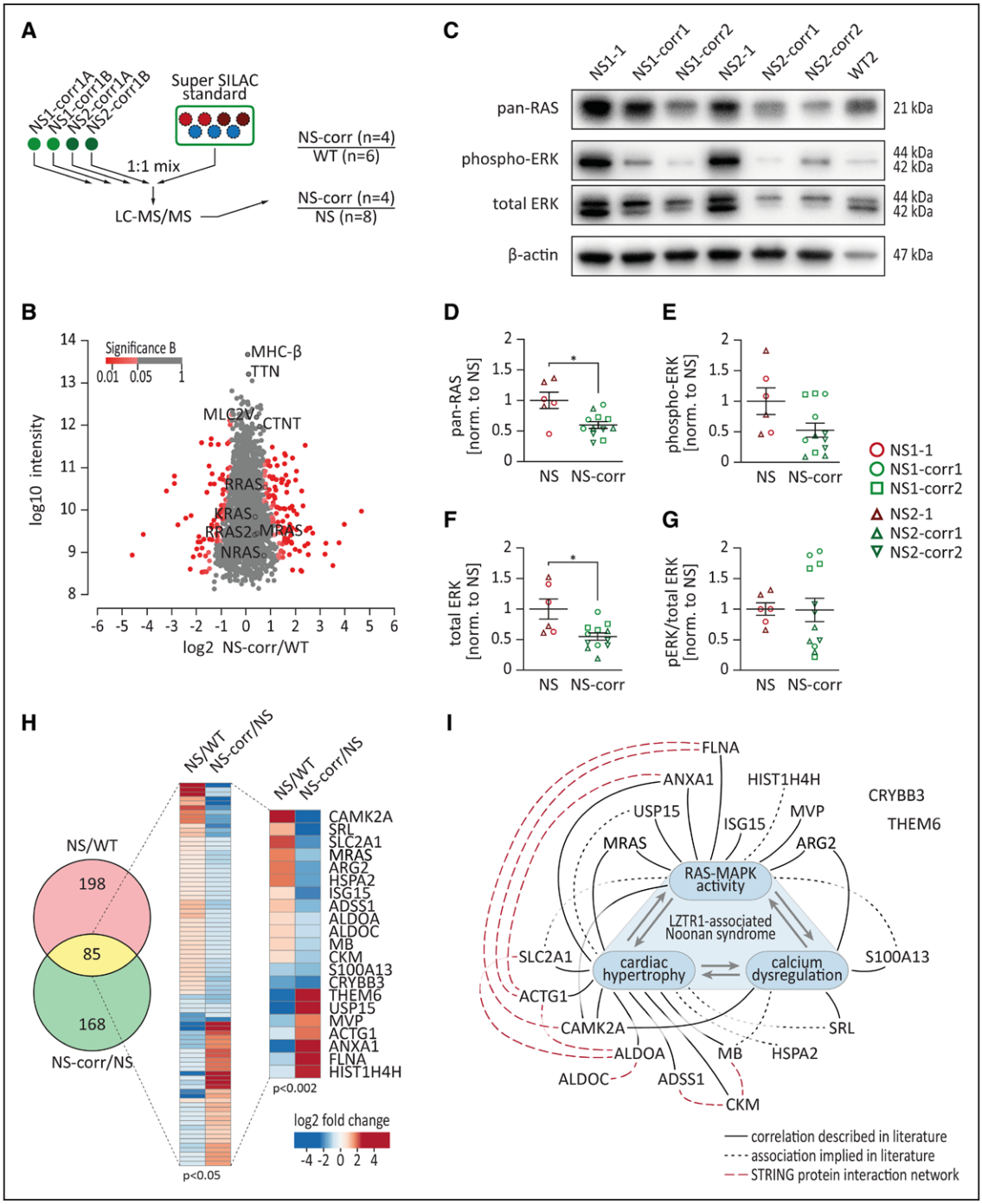

Figure 8. Intronic CRISPR repair normalizes the disease-specific proteome signature.

A, SILAC (Spike-in stable isotope labeling by amino acids in cell culture)–based quantitative proteomics analysis was applied to compare protein expression of CRISPR-repaired iPSC-CMs at days 60 to 75 to datasets obtained from the patients' and WT cultures. Individual samples were processed using the same spike-in super-SILAC standard as in Figure 5 (for WT: n=6 independent differentiations, 3 iPSC lines; for NS: n=8 independent differentiations, 4 iPSC lines, 2 per patient; for NS-corr: n=4 independent differentiations, 2 corrected iPSC lines). **B**, Relative protein abundance between corrected and WT cells. Expression of RAS isoforms in CRISPR-repaired iPSC-CMs was comparable with WT. **C** through **G**, Western blot analysis of RAS-MAPK signaling activity in unstimulated NS, corrected and WT iPSC-CMs at day 60 to 80. **C**, Representative images for RAS, phosphorylated ERK (Thr202/Tyr204 of p44 MAPK and Thr185/Tyr187 of p42 MAPK), total ERK, and housekeeping protein β-actin. Quantitative analyses of (**D**) pan-RAS, (**E**) phosphorylated ERK, (**F**) total ERK, and (**G**) overall ratio of phosphorylated to total ERK protein expression showed decreased abundance of RAS and phosphorylated ERK proteins in corrected compared with NS iPSC-CMs indicating restored LZTR1 function. Data were normalized to total protein and to NS (for NS: n=6 independent differentiations, 2 iPSC lines, 1 per patient; for NS-corr: n=12 independent differentiations, 4 corrected iPSC lines, 2 per patient-derived cell line). **H**, Depiction of disease-relevant proteins detected in SILAC-based proteomics analysis. Comparison of differentially expressed proteins between NS vs WT iPSC-CMs and CRISPR-repaired vs patients' iPSC-CMs revealed an overlap of 85 proteins, most of which showed opposite expression patterns. Overlapping proteins with highest significance ($P<0.002$) are depicted. **I**, Proposed disease-specific proteomic signature of *LZTR1*-associated NS. Several proteins are directly linked to the disease-related features RAS-MAPK activity, cardiac hypertrophy and calcium dysregulation, based on literature research and STRING (Search Tool for the Retrieval of Interacting Genes/Proteins) protein interaction networks. Data are presented as mean±SEM. *$P<0.05$ by nonparametric Mann-Whitney test (**D** through **G**). iPSC-CM indicates induced pluripotent stem cell–derived cardiomyocytes; MAPK, mitogen-activated protein kinase; NS, Noonan syndrome; and WT, wild type.

nonsyndromic HCM,[42,43,64] indicating that *LZTR1*-related HCM has no severe impact on sarcomere structures or myofibril organization. In accordance with an upregulation of genes responsible for calcium handling, our findings demonstrated a dysregulation of calcium homeostasis in the patients' iPSC-CMs. These alterations in calcium cycling are in line with previous studies of HCM models caused by sarcomeric[42,65] as well as RASopathy-associated gene mutations,[31,66] suggesting that both HCM types share common pathways for disease progression. We were able to normalize the dysregulation of CaTs and calcium leak in the NS iPSC-CMs by pharmacological treatment with calcium antagonist verapamil, which is a commonly used drug to treat patients with HCM caused by mutations in sarcomeric genes.[41] However, although disrupted calcium homeostasis is believed to play a central role in the manifestation and progression of cardiac hypertrophy,[65,67] we did not detect a significant attenuation of cellular hypertrophy on long-term treatment with verapamil in vitro. Likewise, long-term MEK inhibition did not normalize CM cell size, although it dramatically reduced RAS-MAPK signaling activity. Collectively, pharmacological intervention (such as calcium channel blockade or MEK inhibition) may prevent some of the phenotypic disease characteristics, but cannot be considered as sustainable therapeutic option for NS-associated HCM.

All currently described NS-associated genes are linked to RAS-MAPK dysregulation with *LZTR1* being the latest gene identified within this pathway.[68] LZTR1 is a member of the BTB-Kelch superfamily, whose members play fundamental roles in various cellular processes such as cell morphology, migration and gene regulation.[69] As *LZTR1* is ubiquitously expressed in various cell types and tissues, dysfunctions of the protein are expected to have a severe impact on diverse cellular processes including cardiac development and CM function. Recent studies elucidated the cellular function of LZTR1 as an adaptor for the cullin 3 ubiquitin ligase complex and identified RAS proteins as its substrates for ubiquitination and subsequent protein degradation.[24–26] By applying SILAC-based quantitative proteomics, as well as Western blot, we were able to show in a disease-related and patient-specific context that LZTR1 dysfunction caused significant accumulation of RAS proteins and consequently led to hyperactivation of RAS-MAPK signaling. Here, particularly MRAS could be identified as a major RAS isoform in human CMs. Our data manifest the importance of LZTR1 in modifying the RAS-MAPK signaling activity in cardiac cells, with its dysfunction leading to accumulation of RAS proteins ultimately resulting in enhanced signaling transduction and development of RASopathy-associated phenotypes.

Although several RASopathy iPSC and mouse models attributed to gain-of-function mutations of the RAS-MAPK pathway have been established,[28,31,66,70,71] the detailed mechanisms by which RAS-MAPK activation engenders the HCM phenotype are not completely understood. Multiple studies revealed that the RAS-MAPK signaling in cross-talk with further pathways such as the calcineurin-NFAT and the PI3K-Akt signaling (multiple other pathways might be involved) together orchestrate the cardiac hypertrophic growth response.[72,73] We were now able to determine a unique disease-specific proteome signature for *LZTR1*-associated NS allowing a deeper analysis of the links between cardiac hypertrophy, abnormal calcium handling and RAS-MAPK hyperactivation, all together provoking the severe phenotype.

To examine whether genomic correction of one of the inherited mutations within *LZTR1* would rescue the disease phenotype in vitro, we performed CRISPR/Cas9 genome editing on the iPSC lines from both patients. The paternal mutation was chosen as a target, as firstly, editing its deep-intronic noncoding location is less likely to result in adverse genomic changes affecting RNA composition. Secondly, insertions or deletions of various sizes introduced by means of nonhomologous end joining would be sufficient to destroy the additional donor splice site created by the intronic mutation (ie, no homology-directed repair is needed which exhibits inherently lower efficiencies, particularly in postmitotic cells). Hence, the correction of the paternal c.1943-256C>T mutation is more feasible to be potentially translated into a clinically relevant genome editing approach.[74,75] Indeed, we were able to eliminate the SNP-induced splice site and thus prevent the inclusion of the cryptic exon into *LZTR1* transcripts by deleting differing numbers of base pairs around the mutation. As a result, we found the cellular hypertrophy detected in the patients' iPSC-CMs now resolved in all CRISPR-repaired cell lines. Moreover, accumulation of RAS proteins and RAS-MAPK signaling activity was normalized in the edited iPSC-CMs.

In correcting the impaired splicing by CRISPR/Cas9-based genome editing, and thereby rescuing the disease phenotype in derived CMs, we provide proof-of-concept for a sustainable therapeutic approach. Since pharmacological treatment was not effective in attenuating the hypertrophic phenotype, we suggest that intronic CRISPR repair of the underlying mutation might be a superior option for the treatment of HCM in *LZTR1*-associated NS. It is well accepted that morbidity and mortality in patients with NS is highly related to the severity of the cardiac phenotype. Therefore, we believe that genetic correction in cardiomyocytes will have an important impact on patients' quality of life.[5] Other congenital symptoms, which cannot be corrected by our strategy, might not play a major role for quality of life (eg, facial dysmorphisms such as hypertelorism and short stature). Whether the described cancer risk in some NS patients could be additionally addressed in the future remains under discussion. Restoration of

deep-intronic mutation-induced protein insufficiency in general could be considered as a therapeutic intervention for various diseases.[76]

So far, HCM in NS has been investigated predominantly in animal models, since primary material from patient samples, especially of pediatric diseases, is only available with considerable difficulty and can only be investigated to a highly restricted extent.[32,77] Our human model described here, demonstrates the potential of iPSC-based technology to model NS in a dish and serves as a highly attractive platform to elucidate the disease mechanisms and evaluate novel therapeutic options. Despite the great advantages of patient-specific iPSC-CMs over previous cardiac models, this study possesses certain limitations. As described by several other reports, iPSC-CMs are developmentally immature and are characterized by gene expression profiles and functional properties similar to fetal CMs.[36,78] However, given the fact that NS is a developmental disorder and that symptoms are often diagnosed prenatally (like in our case report), fetal iPSC-CMs might be especially suitable for studying the disease progression during cardiogenesis. Furthermore, our investigations at single cell and monolayer level are not able to model disease phenotypes at organ level. Finally, multiple mutations in various genes of the RAS-MAPK pathway have been identified to cause NS, and our findings may only be specific to LZTR1 dysfunction.

Taken together, this study revealed the human cardiac pathogenesis in patient-specific iPSC-CMs from NS patients carrying biallelic variants in *LZTR1* and provided a causal link between LZTR1 dysfunction, RAS-MAPK signaling hyperactivity, hypertrophic gene response and cellular hypertrophy. In addition, we identified the intronic CRISPR repair as an option to normalize the hypertrophic phenotype, thereby revealing a personalized and in our view clinically translatable therapeutic strategy.

ARTICLE INFORMATION

Received November 8, 2019; accepted June 15, 2020.

The Data Supplement is available with this article at https://www.ahajournals.org/doi/suppl/10.1161/circulationaha.119.044794.

Authors

Ulrich Hanses, MD; Mandy Kleinsorge, PhD; Lennart Roos, MD; Gökhan Yigit, PhD; Yun Li, MD; Boris Barbarics, MD; Ibrahim El-Battrawy, MD; Huan Lan, MD; Malte Tiburcy, MD; Robin Hindmarsh, MS; Christof Lenz, PhD; Gabriela Salinas, PhD; Sebastian Diecke, PhD; Christian Müller; Ibrahim Adham, PhD; Janine Altmüller, MD; Peter Nürnberg, PhD; Thomas Paul, MD; Wolfram-Hubertus Zimmermann, MD; Gerd Hasenfuss, MD; Bernd Wollnik, MD; Lukas Cyganek, PhD

Correspondence

Lukas Cyganek, PhD, Clinic for Cardiology and Pneumology, University Medical Center Göttingen, Robert-Koch-Str 40, 37075 Göttingen, Germany; or Bernd Wollnik, MD, Institute of Human Genetics, University Medical Center Göttingen, Heinrich-Düker-Weg 12, 37073 Göttingen, Germany. Email Lukas.cyganek@gwdg.de or bernd.wollnik@med.uni-goettingen.de

Affiliations

Clinic for Cardiology and Pneumology (U.H., M.K., L.R., R.H., G.H., L.C.); Institute of Human Genetics (G.Y., Y.L., G.S., C.M., I.A., B.W.); Clinic for Pediatric Cardiology and Intensive Care Medicine (B.B., T.P.); Institute of Pharmacology and Toxicology (M.T., W-H.Z.); Institute for Clinical Chemistry (C.L.), University Medical Center Göttingen, Germany. DZHK (German Center for Cardiovascular Research), partner site Göttingen, Mannheim and Berlin, Germany (U.H., M.K., L.R., G.Y., B.B., I.E-B., M.T., R.H., S.D., T.P., W.-H.Z., G.H., B.W., L.C.). First Department of Medicine, Medical Faculty Mannheim, University Medical Centre Mannheim, University of Heidelberg, Mannheim, Germany (I.E-B., H.L.) Bioanalytical Mass Spectrometry, Max Planck Institute for Biophysical Chemistry, Göttingen, Germany (C.L.). Stem Cell Core Facility, Max Delbrück Center for Molecular Medicine, Berlin, Germany (S.D.). Berlin Institute of Health, Germany (S.D.). Cologne Center for Genomics, University of Cologne, Germany (J.A., P.N.). Cluster of Excellence "Multiscale Bioimaging: from Molecular Machines to Networks of Excitable Cells" (MBExC), University of Göttingen, Germany (W-H.Z., G.H., B.W.).

Acknowledgments

The authors thank Laura Cyganek, Martina Grohe, Yvonne Hintz, Lisa Krebs, Nadine Gotzmann, and Yvonne Wedekind (all Stem Cell Unit, University Medical Center Göttingen), Lisa Neuenroth (Clinical Chemistry, University Medical Center Göttingen), Fabian Ludewig and Orr Shomroni (Human Genetics, University Medical Center Göttingen), and Matthias Simonis for excellent technical assistance. L.C., B.W., and B.B. designed the study. L.C. and B.W. designed the experiments. U.H., M.K., L.R., G.Y., Y.L., I.E.B., H.L., R.H., C.L., G.S., S.D., C.M., I.A., J.A., P.N., B.W., and L.C. performed the experiments and analyzed the data. M.T., T.P., W.H.Z., and G.H. gave technical support and conceptual advice. L.C. and B.W. wrote and M.K. and W.H.Z. edited the manuscript.

Sources of Funding

This work was supported by the German Federal Ministry of Education and Research/German Center for Cardiovascular Research (to L.C., I.E.B., G.H. and W.H.Z.), by the German Research Foundation (CY 90/1-1 to L.C., TI 956/1-1 to M.T., SFB1002 C04, D01, D02, and S01 to M.T., W.-H.Z., G.H., B.W., and L.C., SFB937 TP18 to W.-H.Z., IRTG1816 RP11 to W.-H.Z., EXC 2067/1- 390729940 to W.-H.Z., G.H., and B.W.), and by the German Heart Foundation (to U.H. and L.R.).

Disclosures

None.

Supplemental Materials

Expanded Methods
Data Supplement Figures I–VIII
Data Supplement Tables I–V

REFERENCES

1. Roberts AE, Allanson JE, Tartaglia M, Gelb BD. Noonan syndrome. *Lancet*. 2013;381:333–342. doi: 10.1016/S0140-6736(12)61023-X
2. Binder G, Grathwol S, von Loeper K, Blumenstock G, Kaulitz R, Freiberg C, Webel M, Lissewski C, Zenker M, Paul T. Health and quality of life in adults with Noonan syndrome. *J Pediatr*. 2012;161:501–505.e1. doi: 10.1016/j.jpeds.2012.02.043
3. Mendez HM, Opitz JM. Noonan syndrome. A review. *Am J Med. Genet*. 1985;21:493–506. doi: 10.1002/ajmg.1320210312
4. Hickey EJ, Mehta R, Elmi M, Asoh K, McCrindle BW, Williams WG, Manlhiot C, Benson L. Survival implications: hypertrophic cardiomyopathy in Noonan syndrome. *Congenit Heart Dis*. 2011;6:41–47. doi: 10.1111/j.1747-0803.2010.00465.x
5. Wilkinson JD, Lowe AM, Salbert BA, Sleeper LA, Colan SD, Cox GF, Towbin JA, Connuck DM, Messere JE, Lipshultz SE. Outcomes in children with Noonan syndrome and hypertrophic cardiomyopathy: a study from the Pediatric Cardiomyopathy Registry. *Am Heart J*. 2012;164:442–448. doi: 10.1016/j.ahj.2012.04.018
6. Aoki Y, Niihori T, Inoue S, Matsubara Y. Recent advances in RASopathies. *J Hum Genet*. 2016;61:33–39. doi: 10.1038/jhg.2015.114

7. Simanshu DK, Nissley DV, McCormick F. RAS Proteins and their regulators in human disease. *Cell.* 2017;170:17–33. doi: 10.1016/j.cell.2017.06.009
8. Tartaglia M, Mehler EL, Goldberg R, Zampino G, Brunner HG, Kremer H, van der Burgt I, Crosby AH, Ion A, Jeffery S, et al. Mutations in PTPN11, encoding the protein tyrosine phosphatase SHP-2, cause Noonan syndrome. *Nat Genet.* 2001;29:465–468. doi: 10.1038/ng772
9. Tartaglia M, Pennacchio LA, Zhao C, Yadav KK, Fodale V, Sarkozy A, Pandit B, Oishi K, Martinelli S, Schackwitz W, et al. Gain-of-function SOS1 mutations cause a distinctive form of Noonan syndrome. *Nat Genet.* 2007;39:75–79. doi: 10.1038/ng1939
10. Pandit B, Sarkozy A, Pennacchio LA, Carta C, Oishi K, Martinelli S, Pogna EA, Schackwitz W, Ustaszewska A, Landstrom A, et al. Gain-of-function RAF1 mutations cause Noonan and LEOPARD syndromes with hypertrophic cardiomyopathy. *Nat Genet.* 2007;39:1007–1012. doi: 10.1038/ng2073
11. Razzaque MA, Nishizawa T, Komoike Y, Yagi H, Furutani M, Amo R, Kamisago M, Momma K, Katayama H, Nakagawa M, et al. Germline gain-of-function mutations in RAF1 cause Noonan syndrome. *Nat Genet.* 2007;39:1013–1017. doi: 10.1038/ng2078
12. Aoki Y, Niihori T, Banjo T, Okamoto N, Mizuno S, Kurosawa K, Ogata T, Takada F, Yano M, Ando T, et al. Gain-of-function mutations in RIT1 cause Noonan syndrome, a RAS/MAPK pathway syndrome. *Am J Hum Genet.* 2013;93:173–180. doi: 10.1016/j.ajhg.2013.05.021
13. Schubbert S, Zenker M, Rowe SL, Böll S, Klein C, Bollag G, van der Burgt I, Musante L, Kalscheuer V, Wehner LE, et al. Germline KRAS mutations cause Noonan syndrome. *Nat Genet.* 2006;38:331–336. doi: 10.1038/ng1748
14. Cirstea IC, Kutsche K, Dvorsky R, Gremer L, Carta C, Horn D, Roberts AE, Lepri F, Merbitz-Zahradnik T, König R, et al. A restricted spectrum of NRAS mutations causes Noonan syndrome. *Nat Genet.* 2010;42:27–29. doi: 10.1038/ng.497
15. Flex E, Jaiswal M, Pantaleoni F, Martinelli S, Strullu M, Fansa EK, Caye A, De Luca A, Lepri F, Dvorsky R, et al. Activating mutations in RRAS underlie a phenotype within the RASopathy spectrum and contribute to leukaemogenesis. *Hum Mol Genet.* 2014;23:4315–4327. doi: 10.1093/hmg/ddu148
16. Cordeddu V, Di Schiavi E, Pennacchio LA, Ma'ayan A, Sarkozy A, Fodale V, Cecchetti S, Cardinale A, Martin J, Schackwitz W, et al. Mutation of SHOC2 promotes aberrant protein N-myristoylation and causes Noonan-like syndrome with loose anagen hair. *Nat Genet.* 2009;41:1022–1026. doi: 10.1038/ng.425
17. Gripp KW, Aldinger KA, Bennett JT, Baker L, Tusi J, Powell-Hamilton N, Stabley D, Sol-Church K, Timms AE, Dobyns WB. A novel rasopathy caused by recurrent de novo missense mutations in PPP1CB closely resembles Noonan syndrome with loose anagen hair. *Am J Med. Genet A.* 2016;170:2237–2247. doi: 10.1002/ajmg.a.37781
18. Martinelli S, De Luca A, Stellacci E, Rossi C, Checquolo S, Lepri F, Caputo V, Silvano M, Buscherini F, Consoli F, et al. Heterozygous germline mutations in the CBL tumor-suppressor gene cause a Noonan syndrome-like phenotype. *Am J Hum Genet.* 2010;87:250–257. doi: 10.1016/j.ajhg.2010.06.015
19. Chen PC, Yin J, Yu HW, Yuan T, Fernandez M, Yung CK, Trinh QM, Peltekova VD, Reid JG, Tworog-Dube E, et al. Next-generation sequencing identifies rare variants associated with Noonan syndrome. *Proc Natl Acad Sci U S A.* 2014;111:11473–11478. doi: 10.1073/pnas.1324128111
20. Piotrowski A, Xie J, Liu YF, Poplawski AB, Gomes AR, Madanecki P, Fu C, Crowley MR, Crossman DK, Armstrong L, et al. Germline loss-of-function mutations in LZTR1 predispose to an inherited disorder of multiple schwannomas. *Nat Genet.* 2014;46:182–187. doi: 10.1038/ng.2855
21. Frattini V, Trifonov V, Chan JM, Castano A, Lia M, Abate F, Keir ST, Ji AX, Zoppoli P, Niola F, et al. The integrated landscape of driver genomic alterations in glioblastoma. *Nat Genet.* 2013;45:1141–1149. doi: 10.1038/ng.2734
22. Yamamoto GL, Aguena M, Gos M, Hung C, Pilch J, Fahiminiya S, Abramowicz A, Cristian I, Buscarilli M, Naslavsky MS, et al. Rare variants in SOS2 and LZTR1 are associated with Noonan syndrome. *J Med Genet.* 2015;52:413–421. doi: 10.1136/jmedgenet-2015-103018
23. Johnston JJ, van der Smagt JJ, Rosenfeld JA, Pagnamenta AT, Alswaid A, Baker EH, Blair E, Borck G, Brinkmann J, Craigen W, et al; Members of the Undiagnosed Diseases Network. Autosomal recessive Noonan syndrome associated with biallelic LZTR1 variants. *Genet Med.* 2018;20:1175–1185. doi: 10.1038/gim.2017.249
24. Bigenzahn JW, Collu GM, Kartnig F, Pieraks M, Vladimer GI, Heinz LX, Sedlyarov V, Schischlik F, Fauster A, Rebsamen M, et al. LZTR1 is a regulator of RAS ubiquitination and signaling. *Science.* 2018;362:1171–1177. doi: 10.1126/science.aap8210
25. Steklov M, Pandolfi S, Baietti MF, Batiuk A, Carai P, Najm P, Zhang M, Jang H, Renzi F, Cai Y, et al. Mutations in LZTR1 drive human disease by dysregulating RAS ubiquitination. *Science.* 2018;362:1177–1182. doi: 10.1126/science.aap7607
26. Castel P, Cheng A, Cuevas-Navarro A, Everman DB, Papageorge AG, Simanshu DK, Tankka A, Galeas J, Urisman A, McCormick F. RIT1 oncoproteins escape LZTR1-mediated proteolysis. *Science.* 2019;363:1226–1230. doi: 10.1126/science.aav1444
27. Robinton DA, Daley GQ. The promise of induced pluripotent stem cells in research and therapy. *Nature.* 2012;481:295–305. doi: 10.1038/nature10761
28. Jaffré F, Miller CL, Schänzer A, Evans T, Roberts AE, Hahn A, Kontaridis MI. Inducible pluripotent stem cell-derived cardiomyocytes reveal aberrant extracellular regulated kinase 5 and mitogen-activated protein kinase kinase ½ signaling concomitantly promote hypertrophic vardiomyopathy in RAF1-sssociated Noonan syndrome. *Circulation.* 2019;140:207–224. doi: 10.1161/CIRCULATIONAHA.118.037227
29. Carvajal-Vergara X, Sevilla A, D'Souza SL, Ang YS, Schaniel C, Lee DF, Yang L, Kaplan AD, Adler ED, Rozov R, et al. Patient-specific induced pluripotent stem-cell-derived models of LEOPARD syndrome. *Nature.* 2010;465:808–812. doi: 10.1038/nature09005
30. Rooney GE, Goodwin AF, Depeille P, Sharir A, Schofield CM, Yeh E, Roose JP, Klein OD, Rauen KA, Weiss LA, et al. Human iPS cell-derived neurons uncover the impact of increased Ras signaling in Costello Syndrome. *J Neurosci.* 2016;36:142–152. doi: 10.1523/JNEUROSCI.1547-15.2016
31. Josowitz R, Mulero-Navarro S, Rodriguez NA, Falce C, Cohen N, Ullian EM, Weiss LA, Rauen KA, Sobie EA, Gelb BD. Autonomous and non-autonomous defects underlie hypertrophic cardiomyopathy in BRAF-mutant hiPSC-derived cardiomyocytes. *Stem Cell Reports.* 2016;7:355–369. doi: 10.1016/j.stemcr.2016.07.018
32. Sayed N, Liu C, Wu JC. Translation of human-induced pluripotent stem cells: from clinical trial in a dish to precision medicine. *J Am Coll Cardiol.* 2016;67:2161–2176. doi: 10.1016/j.jacc.2016.01.083
33. Eschenhagen T, Mummery C, Knollmann BC. Modelling sarcomeric cardiomyopathies in the dish: from human heart samples to iPSC cardiomyocytes. *Cardiovasc Res.* 2015;105:424–438. doi: 10.1093/cvr/cvv017
34. Hockemeyer D, Jaenisch R. Induced pluripotent stem cells meet genome editing. *Cell Stem Cell.* 2016;18:573–586. doi: 10.1016/j.stem.2016.04.013
35. Long C, Li H, Tiburcy M, Rodriguez-Caycedo C, Kyrychenko V, Zhou H, Zhang Y, Min YL, Shelton JM, Mammen PPA, et al. Correction of diverse muscular dystrophy mutations in human engineered heart muscle by single-site genome editing. *Sci Adv.* 2018;4:eaap9004. doi: 10.1126/sciadv.aap9004
36. Cyganek L, Tiburcy M, Sekeres K, Gerstenberg K, Bohnenberger H, Lenz C, Henze S, Stauske M, Salinas G, Zimmermann W-H, et al. Deep phenotyping of human induced pluripotent stem cell-derived atrial and ventricular cardiomyocytes. *JCI Insight*. 2018;3:99941. doi: 10.1172/jci.insight.99941
37. El-Battrawy I, Lan H, Cyganek L, Zhao Z, Li X, Buljubasic F, Lang S, Yücel G, Sattler K, Zimmermann W-H, et al. Modeling short QT syndrome using human-induced pluripotent stem cell-derived cardiomyocytes. *J Am Heart Assoc.* 2018;7:e007394. doi: 10.1161/JAHA.117.007394
38. Lindeboom RG, Supek F, Lehner B. The rules and impact of nonsense-mediated mRNA decay in human cancers. *Nat Genet.* 2016;48:1112–1118. doi: 10.1038/ng.3664
39. Man J, Barnett P, Christoffels VM. Structure and function of the Nppa-Nppb cluster locus during heart development and disease. *Cell Mol Life Sci.* 2018;75:1435–1444. doi: 10.1007/s00018-017-2737-0
40. Sala L, van Meer BJ, Tertoolen LGJ, Bakkers J, Bellin M, Davis RP, Denning C, Dieben MAE, Eschenhagen T, Giacomelli E, et al. MUSCLEMOTION: a versatile open software tool to quantify cardiomyocyte and cardiac muscle contraction in vitro and in vivo. *Circ Res.* 2018;122:e5–e16. doi: 10.1161/CIRCRESAHA.117.312067
41. Elliott PM, Anastasakis A, Borger MA, Borggrefe M, Cecchi F, Charron P, Hagege AA, Lafont A, Limongelli G, Mahrholdt H, et al. 2014 ESC Guidelines on diagnosis and management of hypertrophic cardiomyopathy. The Task Force for the Diagnosis and Management of Hypertrophic Cardiomyopathy of the European Society of Cardiology (ESC). *Eur Heart J.* 2014;35:2733–2779. doi: 10.1093/eurheartj/ehu284
42. Lan F, Lee AS, Liang P, Sanchez-Freire V, Nguyen PK, Wang L, Han L, Yen M, Wang Y, Sun N, et al. Abnormal calcium handling properties underlie familial hypertrophic cardiomyopathy pathology in patient-specific

induced pluripotent stem cells. *Cell Stem Cell.* 2013;12:101–113. doi: 10.1016/j.stem.2012.10.010
43. Mosqueira D, Mannhardt I, Bhagwan JR, Lis-Slimak K, Katili P, Scott E, Hassan M, Prondzynski M, Harmer SC, Tinker A, et al. CRISPR/Cas9 editing in human pluripotent stem cell-cardiomyocytes highlights arrhythmias, hypocontractility, and energy depletion as potential therapeutic targets for hypertrophic cardiomyopathy. *Eur Heart J.* 2018;39:3879–3892. doi: 10.1093/eurheartj/ehy249
44. Wu H, Yang H, Rhee JW, Zhang JZ, Lam CK, Sallam K, Chang ACY, Ma N, Lee J, Zhang H, et al. Modelling diastolic dysfunction in induced pluripotent stem cell-derived cardiomyocytes from hypertrophic cardiomyopathy patients. *Eur Heart J.* 2019;40:3685–3695. doi: 10.1093/eurheartj/ehz326
45. Husum D, Johnsen A, Jensen G. Requirements for drug monitoring of verapamil: experience from an unselected group of patients with cardiovascular disease. *Pharmacol Toxicol.* 1990;66:163–169. doi: 10.1111/j.1600-0773.1990.tb00726.x
46. Geiger T, Wisniewski JR, Cox J, Zanivan S, Kruger M, Ishihama Y, Mann M. Use of stable isotope labeling by amino acids in cell culture as a spike-in standard in quantitative proteomics. *Nat Protoc.* 2011;6:147–157. doi: 10.1038/nprot.2010.192
47. Higgins EM, Bos JM, Mason-Suares H, Tester DJ, Ackerman JP, MacRae CA, Sol-Church K, Gripp KW, Urrutia R, Ackerman MJ. Elucidation of MRAS-mediated Noonan syndrome with cardiac hypertrophy. *JCI Insight.* 2017;2:e91225. doi: 10.1172/jci.insight.91225
48. Motta M, Sagi-Dain L, Krumbach OHF, Hahn A, Peleg A, German A, Lissewski C, Coppola S, Pantaleoni F, Kocherscheid L, et al. Activating MRAS mutations cause Noonan syndrome associated with hypertrophic cardiomyopathy. *Hum Mol Genet*. 2019;ddz108. doi: 10.1093/hmg/ddz108
49. Yeung T-L, Tsai CC, Leung CS, Au Yeung C-L, Thompson MS, Lu KH, Freedman RS, Birrer MJ, Wong K-K, Mok SC. ISG15 promotes ERK1 ISGylation, CD8+ T cell activation and suppresses ovarian cancer progression. *Cancers (Basel)*. 2018;10:464. doi: 10.3390/cancers10120464
50. Burks J, Reed RE, Desai SD. ISGylation governs the oncogenic function of Ki-Ras in breast cancer. *Oncogene.* 2014;33:794–803. doi: 10.1038/onc.2012.633
51. Hayes SD, Liu H, MacDonald E, Sanderson CM, Coulson JM, Clague MJ, Urbé S. Direct and indirect control of mitogen-activated protein kinase pathway-associated components, BRAP/IMP E3 ubiquitin ligase and CRAF/RAF1 kinase, by the deubiquitylating enzyme USP15. *J Biol Chem.* 2012;287:43007–43018. doi: 10.1074/jbc.M112.386938
52. Alldridge LC, Harris HJ, Plevin R, Hannon R, Bryant CE. The annexin protein lipocortin 1 regulates the MAPK/ERK pathway. *J Biol Chem.* 1999;274:37620–37628. doi: 10.1074/jbc.274.53.37620
53. Yang YH, Toh M-L, Clyne CD, Leech M, Aeberli D, Xue J, Dacumos A, Sharma L, Morand EF. Annexin 1 negatively regulates IL-6 expression via effects on p38 MAPK and MAPK phosphatase-1. *J Immunol*. 2006;177:8148–8153. doi: 10.4049/jimmunol.177.11.8148
54. Cipolletta E, Rusciano MR, Maione AS, Santulli G, Sorriento D, Del Giudice C, Ciccarelli M, Franco A, Crola C, Campiglia P, et al. Targeting the CaMKII/ERK interaction in the heart prevents cardiac hypertrophy. *PLoS One.* 2015;10:e0130477. doi: 10.1371/journal.pone.0130477
55. Mollova MY, Katus HA, Backs J. Regulation of CaMKII signaling in cardiovascular disease. *Front Pharmacol.* 2015;6:178. doi: 10.3389/fphar.2015.00178
56. Shimura M, Minamisawa S, Takeshima H, Jiao Q, Bai Y, Umemura S, Ishikawa Y. Sarcalumenin alleviates stress-induced cardiac dysfunction by improving Ca2+ handling of the sarcoplasmic reticulum. *Cardiovasc Res.* 2008;77:362–370. doi: 10.1093/cvr/cvm019
57. Jiao Q, Bai Y, Akaike T, Takeshima H, Ishikawa Y, Minamisawa S. Sarcalumenin is essential for maintaining cardiac function during endurance exercise training. *Am J Physiol Heart Circ Physiol.* 2009;297:H576–H582. doi: 10.1152/ajpheart.00946.2008
58. Morissette MR, Howes AL, Zhang T, Heller Brown J. Upregulation of GLUT1 expression is necessary for hypertrophy and survival of neonatal rat cardiomyocytes. *J Mol Cell Cardiol.* 2003;35:1217–1227. doi: 10.1016/s0022-2828(03)00212-8
59. Montessuit C, Thorburn A. Transcriptional activation of the glucose transporter GLUT1 in ventricular cardiac myocytes by hypertrophic agonists. *J Biol Chem.* 1999;274:9006–9012. doi: 10.1074/jbc.274.13.9006
60. Wen HY, Xia Y, Young ME, Taegtmeyer H, Kellems RE. The adenylosuccinate synthetase-1 gene is activated in the hypertrophied heart. *J Cell Mol Med.* 2002;6:235–243. doi: 10.1111/j.1582-4934.2002.tb00190.x
61. Li Y, Zhang D, Kong L, Shi H, Tian X, Gao L, Liu Y, Wu L, Du B, Huang Z, et al. Aldolase promotes the development of cardiac hypertrophy by targeting AMPK signaling. *Exp Cell Res*. 2018;370:78–86. doi: 10.1016/j.yexcr.2018.06.009
62. Pagani F, Baralle FE. Genomic variants in exons and introns: identifying the splicing spoilers. *Nat Rev Genet.* 2004;5:389–396. doi: 10.1038/nrg1327
63. Lewandowska MA. The missing puzzle piece: splicing mutations. *Int J Clin Exp Pathol.* 2013;6:2675–2682.
64. Han L, Li Y, Tchao J, Kaplan AD, Lin B, Li Y, Mich-Basso J, Lis A, Hassan N, London B, et al. Study familial hypertrophic cardiomyopathy using patient-specific induced pluripotent stem cells. *Cardiovasc Res.* 2014;104:258–269. doi: 10.1093/cvr/cvu205
65. Fatkin D, McConnell BK, Mudd JO, Semsarian C, Moskowitz IG, Schoen FJ, Giewat M, Seidman CE, Seidman JG. An abnormal Ca(2+) response in mutant sarcomere protein-mediated familial hypertrophic cardiomyopathy. *J Clin Invest.* 2000;106:1351–1359. doi: 10.1172/JCI11093
66. Clay SA, Domeier TL, Hanft LM, McDonald KS, Krenz M. Elevated Ca2+ transients and increased myofibrillar power generation cause cardiac hypercontractility in a model of Noonan syndrome with multiple lentigines. *Am J Physiol Heart Circ Physiol.* 2015;308:H1086–H1095. doi: 10.1152/ajpheart.00501.2014
67. Robinson P, Liu X, Sparrow A, Patel S, Zhang YH, Casadei B, Watkins H, Redwood C. Hypertrophic cardiomyopathy mutations increase myofilament Ca2+ buffering, alter intracellular Ca2+ handling, and stimulate Ca2+-dependent signaling. *J Biol Chem.* 2018;293:10487–10499. doi: 10.1074/jbc.RA118.002081
68. Tidyman WE, Rauen KA. Pathogenetics of the RASopathies. *Hum Mol Genet.* 2016;25(R2):R123–R132. doi: 10.1093/hmg/ddw191
69. Adams J, Kelso R, Cooley L. The kelch repeat superfamily of proteins: propellers of cell function. *Trends Cell Biol.* 2000;10:17–24. doi: 10.1016/s0962-8924(99)01673-6
70. Wu X, Simpson J, Hong JH, Kim K-H, Thavarajah NK, Backx PH, Neel BG, Araki T. MEK-ERK pathway modulation ameliorates disease phenotypes in a mouse model of Noonan syndrome associated with the Raf1(L613V) mutation. *J Clin Invest*. 2011;121:1009–1025. doi: 10.1172/JCI44929
71. Marin TM, Keith K, Davies B, Conner DA, Guha P, Kalaitzidis D, Wu X, Lauriol J, Wang B, Bauer M, et al. Rapamycin reverses hypertrophic cardiomyopathy in a mouse model of LEOPARD syndrome-associated PTPN11 mutation. *J Clin Invest.* 2011;121:1026–1043. doi: 10.1172/JCI44972
72. Molkentin JD. Calcineurin-NFAT signaling regulates the cardiac hypertrophic response in coordination with the MAPKs. *Cardiovasc Res.* 2004;63:467–475. doi: 10.1016/j.cardiores.2004.01.021
73. Mutlak M, Kehat I. Extracellular signal-regulated kinases ½ as regulators of cardiac hypertrophy. *Front Pharmacol.* 2015;6:149. doi: 10.3389/fphar.2015.00149
74. Amoasii L, Hildyard JCW, Li H, Sanchez-Ortiz E, Mireault A, Caballero D, Harron R, Stathopoulou TR, Massey C, Shelton JM, et al. Gene editing restores dystrophin expression in a canine model of Duchenne muscular dystrophy. *Science.* 2018;362:86–91. doi: 10.1126/science.aau1549
75. Maeder ML, Stefanidakis M, Wilson CJ, Baral R, Barrera LA, Bounoutas GS, Bumcrot D, Chao H, Ciulla DM, DaSilva JA, et al. Development of a gene-editing approach to restore vision loss in Leber congenital amaurosis type 10. *Nat Med.* 2019;25:229–233. doi: 10.1038/s41591-018-0327-9
76. Vaz-Drago R, Custódio N, Carmo-Fonseca M. Deep intronic mutations and human disease. *Hum Genet.* 2017;136:1093–1111. doi: 10.1007/s00439-017-1809-4
77. Gintant G, Fermini B, Stockbridge N, Strauss D. The evolving roles of human iPSC-derived cardiomyocytes in drug safety and discovery. *Cell Stem Cell.* 2017;21:14–17. doi: 10.1016/j.stem.2017.06.005
78. Yang X, Pabon L, Murry CE. Engineering adolescence: maturation of human pluripotent stem cell-derived cardiomyocytes. *Circ Res.* 2014;114:511–523. doi: 10.1161/CIRCRESAHA.114.300558